

Non-equilibrium spin dynamics in the temperature and magnetic field dependence of magnetization curves of ferrimagnetic $\text{Co}_{1.75}\text{Fe}_{1.25}\text{O}_4$ and its composite with BaTiO_3

R.N. Bhowmik^{*1}, and R.Ranganathan²

¹Department of Physics, Pondicherry University, R. V Nagar, Kalapet, Pondicherry-605014, India.

Condensed Matter Physics Division, Saha Institute of Nuclear Physics, 1/AF Bidhannagar, Kolkata-700064

*Corresponding author: Tel.: +91-9944064547; E-mail: rnbhowmik.phy@pondiuni.edu.in

Abstract

A composite material has been prepared by high temperature heating of the mixed powders of ferrimagnetic $\text{Co}_{1.75}\text{Fe}_{1.25}\text{O}_4$ (CFO) spinel oxide and non-magnetic BaTiO_3 (BTO) particles. The mixture of CFO and BTO structures has been confirmed by synchrotron X-Ray diffraction. The basic properties of ferrimagnetic CFO sample have been retained in the composite. However, a remarkable modification in magnetic spin dynamics arises due to interfacial effect. The blocking phenomenon of ferrimagnetic domains below the room temperature has been tuned by varying the modes of (zero field cooled and field cooled) measurements and magnitude of magnetic fields. The non-equilibrium dynamics of magnetic spin order has been examined by adopting unconventional protocols during recording of time dependent magnetization at different stages of the temperature and field dependence of magnetization curves. The magnetic relaxation followed exponential equation with two time constants. There are certain cases, where slow spin dynamics followed logarithmic function of time. The incorporation of off-field relaxation experiments has made possible to tune magnetic state and coercivity of the material. The systems showed various novel phenomena, including meta-stable magnetic state, exchange bias effect, memory effect and training effect, which are of current interest for device applications of the magnetic materials.

Keywords: Spinel ferrite, Composite magnet, Domain wall pinning, Magnetic relaxation.

1. Introduction

Spinel ferrites are defined by the general formula unit AB_2O_4 , where metal ions occupy the tetrahedral (A) and octahedral (B) coordinated lattice sites with anions (O^{2-}) at fcc positions of lattice structure [1-2]. The local ordering of the 3d electronic spins of Co and Fe ions in doubly and triply degenerated e_g and t_{2g} levels of octahedral sites control the magnetic spin moment in spinel structure. Each Co^{2+} ion at A sites contains three unpaired electrons at t_{2g} level and at B sites contains one unpaired electron at t_{2g} level and two unpaired electrons at e_g level, respectively. Each A site or B site Fe^{3+} ion contains five unpaired electrons at e_g and t_{2g} level. On the other hand, each Co^{3+} ion at B sites results nearly zero moment. So, magnetic moment in defect free spinel structure is determined by the site exchange of Fe^{3+} ($\sim 3.91 \mu_B$) and Co^{2+} ($\sim 2.52 \mu_B$) ions. The distribution of anisotropy and superexchange interactions ($J(A-O-B)$, ($J(B-O-B)$), ($J(A-O-A)$) between magnetic ions at A and B sites affect the magnetic properties in spinel structure. In a long range ferrimagnetic structure, antiferromagnetic (AFM) superexchange interactions between A and B site moments ($J(A-O-B)$) are expected to be strong in comparison to intra-sublattice interactions ($J(B-O-B)$ and ($J(A-O-A)$). The variation of relative strengths and competition between exchange interactions, and differences in electronic spin order of ions in the ferrimagnetic domains can introduce magnetic spin disorder in magnetic spinel oxides [3-5].

In addition to intrinsic spin disorder and frustration in magnetic materials, the interfacial magnetic exchange interactions in hetero-structured systems have shown many novel magnetic phenomena, e.g., blocking of magnetic domains, domain wall pinning, exchange bias, training effect, and memory effect [6-13]. The exchange bias effect was primarily modeled for FM and AFM layers of thin films [3-4]. However, exchange bias effect has been found in particulate systems, where interfacial exchange coupling has been modeled between core-shell structure of

FM and weak FM/AFM layers [13-14]. The memory effect was observed in non-equilibrium spin systems that have strong inter-particle interactions and meta-stable energy states [15]. It is characterized by ageing effects. The training effect, on the other hand, originates from an irreversible change in the pinned spin structure at domain walls or at the interfaces of FM-AFM structure of materials or at the interfaces of ferromagnetic and ferroelectric systems [9, 16-17]. Interestingly, magnetic memory effect dominates at higher temperatures in comparison to the observation of exchange bias effect at lower temperatures [12, 15, 18]. The understanding of non-equilibrium magnetic phenomena are useful for applications of magnetic materials in spin valves, spins filter, read-writing devices, magneto-resistive random access memories, sensors and magnetic switches [19-20]. This requires an effective strategy for revealing the existence of intrinsic spin disorder and distribution of local anisotropies and exchange interactions inside the domains or at the interfaces of composite materials [9].

In this work, we demonstrate the effects of intrinsic magnetic disorder in ferrimagnetic $\text{Co}_{1.75}\text{Fe}_{1.25}\text{O}_4$ spinel oxide [21] and extrinsic magnetic disorder in its composite with non-magnetic BaTiO_3 [22]. The intrinsic spin disorder in the spinel oxide is expected due to replacement of a fraction of the Fe^{3+} (high spin state) ions at B sites by the non-magnetic (low spin) Co^{3+} ions and random exchange of the remaining magnetic ions (Co^{2+} (highly anisotropic) and Fe^{3+} (less anisotropic)) between A and B sites. Thermodynamically, the present spinel oxide stabilizes in single phase only at annealing temperature around 900 °C. Otherwise, structural instability of the atoms at B sites produces spinodal decomposition of Co- and Fe-rich phases (self-composite structure) [23-24]. Interestingly, structural phase instability of the $\text{Co}_{1.75}\text{Fe}_{1.25}\text{O}_4$ ferrite has been reduced in its composite with BaTiO_3 (ferroelectric and non-magnetic) [22]. However, extrinsic disorder is modified in the composite due to lattice mismatch at the interfaces

of coexisting two different structural and magnetic phases [25]. Hence, an in-depth study of the non-equilibrium magnetic spin dynamics has been carried out at temperatures below the magnetic blocking temperature to understand the effect of distribution of magnetic exchange interactions in pure and composite form of magnetic spinel oxides.

2. Experimental

The material preparation and characterization of the $\text{Co}_{1.75}\text{Fe}_{1.25}\text{O}_4$ (CFO) ferrite and its composite with BaTiO_3 (BTO) were described in earlier works [21-22]. The as prepared ferrite powder after chemical reaction was made into pellet and thermally annealed at different temperatures (200-1100 °C) for 2 hrs. The sample CF90 was obtained by annealing the as-prepared ferrite powder at 900 °C. It formed single phase cubic spinel structure. Otherwise, the as-prepared sample after annealing at different temperatures (e.g., CF80 sample with annealing temperature at 800 °C) formed bi-phased cubic spinel structure. The composite sample CF80_BTO was prepared by mixing the CF80 ferrite and BTO powders with mass ratio 50:50, and final heating at 1000 °C for 4 hrs. Synchrotron X-ray diffraction pattern of the composite CF80_BTO sample confirmed the coexistence of cubic spinel structured CFO and tetragonal phase of BTO without any intermediate phase formation.

Magnetic measurements were carried out using Physical property measurement system (PPMS-EC2, Quantum Design, USA). We used some unconventional protocols for examining the time response of the non-equilibrium magnetic state during temperature and magnetic field dependence of magnetization measurements. The temperature dependence of magnetization was recorded using zero field cooled (ZFC) and field cooled (FC) modes with conventional and unconventional protocols (PCs). The protocol 1 (PC1) is a conventional ZFC mode (Fig. 1(a)), where the sample was cooled from 300/330 K to 10 K in the absence of external magnetic field

or applying a small field to maintain the residual magnetization close to zero during cooling process. This is followed by measurement of magnetization at set (constant) magnetic field while temperature of the sample is warming up to 300 K/340 K. The protocol 2 (PC2) is the conventional FC mode (Fig. 1(b)), where the sample was cooled from 300/340 K to 10 K in the presence of constant external magnetic field. The magnetization was recorded during cooling process from higher temperature (MFCC (T) mode) or the sample was first field cooled down to 10 K without recording the magnetization and magnetization was recorded during increase of the temperature from 10 K to 300 K without changing the cooling field (MFCW (T) mode).

Apart from above conventional MZFC(T) and MFC(T) modes, the non-equilibrium spin dynamics of the samples were examined by following various protocols for recording magnetic data $M(T, H, t_w)$ during waiting time (t_w). The protocol 3 (PC3) is the unconventional $M(T, H = \text{OFF}, t_w)$ mode (Fig. 1(c)), where the sample was cooled using MFCC(T) mode with intermediate cooling field off for time (t_w) at 250 K, 150 K and 50 K. The $M(t_w)$ data were recorded before making the cooling field once again to ON condition and resuming the MFCC(T) measurement on lowering the temperature. The protocol 4 (PC4) is the unconventional $M(T, H = \text{ON}, t_w)$ mode (Fig. 1(d)), where the sample was first zero field cooled down to 10 K. This was followed by application of a set magnetic field at selected temperatures for waiting time t_w while sample temperature was increasing and $M(t_w)$ data were recorded during waiting time. After recording $M(t_w)$ data, applied field was made into zero and the sample was moved up to next measurement temperature in the absence of magnetic field. The protocol 5 (PC5) is the conventional field dependence of magnetization ($M(H)$) measurement (Fig. 1(e)), where $M(H)$ curve was recorded at set temperatures after zero field cooling or field cooling of the sample from 330 K in the presence of magnetic field, typically 50/70 kOe. The protocol 6 (PC6) is the unconventional M

($T = \text{constant}$, H , t_w) measurement (Fig. 1(f)), where the sample was either zero field cooled or field cooled from 300 K to the set temperature. The measurement of $M(H)$ curve was recorded by varying the field from +70 kOe/-70 kOe with an intermediate halting of $M(H)$ measurement for time (t_w) at fields just before the coercive field points on negative/positive axis and $M(t_w)$ data were recorded during t_w . After $M(t_w)$ measurement, the $M(H)$ measurement was continued by sweeping the magnetic field.

3. Results and discussion

3.1. Temperature and field dependent magnetization [$M(T,H, t_w)$] for CF90 sample

Fig. 2(a) plots the MZFC(T) and MFCW(T) curves at +500 Oe, measured using protocols PC1 and PC2. The MZFC(T) curve exhibits magnetic blocking temperature (T_m) at about 300 K or above. A wide bifurcation between MFCW(T) and MZFC(T) curves below T_m suggests highly anisotropic character of the sample depending on cooling process. A rapid decrease of the MZFC curve below blocking temperature and nearly temperature independent nature below 150 K at low fields indicates domain-wall pinning effect [26]. The MZFC(T) curves in Fig. 2(b) showed more or less symmetric responses for positive and negative fields up to ± 2 kOe about the zero magnetization line. The magnitude of MZFC(T) curve increased with a shift of the peak position to lower temperature on increasing the magnetic field, but MZFC(T) curves below 150 K are not significantly affected by the increase of magnetic field up to ± 2 kOe. This means Zeeman energy ($K_H = -M_{\text{sat}} H \cos(\theta - \varphi)$) at low fields is not enough to overcome the anisotropy energy ($K_A = K_{\text{eff}}(T) \sin^2\theta$) of the sample at low temperature [9]. A broad peak in the MZFC(T) curves qualitatively describes a distribution of anisotropy inside the magnetic domains or at the interfaces of domains/particles. The distribution of anisotropy energy can be quantified from first order derivative of the MZFC(T) curves (Fig. 2(c)). The peak (T_p) of the dM/dT vs. T curve

corresponds to the inflection point of the MZFC(T) curve below T_m . The peak profile in the dM/dT vs. T curves (Fig. 2(d-e)) was fitted with Lorentzian shape to determine the peak parameters. The intercept of the dM/dT curve on temperature axis ($> T_p$) defines the blocking temperature (T_m). Fig. 2(f) shows a symmetrically decrease of the peak parameters (T_p , width, T_m) about the zero point of magnetic field axis with the increase of field magnitude. The increase of peak height arises due to field induced clustering of the magnetic domains/particles [15].

Fig. 3(a) demonstrates magnetic memory effect in pure ferrite sample. The memory effect was tested using protocol PC2. The MFCC(T) curve was measured at 200 Oe during decrease of the temperature from 300 K to 250 K. At 250 K, the field was made to zero and magnetization was recorded in the off-field condition during waiting time (t_w) 1500 s. Then, field +200 Oe was made on at 250 K and MFCC(T) measurement continued till the temperature reached down to 150 K. Similar steps were followed to record the magnetization during waiting time (t_w) 1500 s at 150 K and also at 50 K. Finally, MFCC(T) measurement at +200 Oe was continued down to 10 K. Next, MFCW(T) curve was recorded during increase of the temperature from 10 K to 300 K without changing the cooling field +200 Oe and without any intermediate waiting at 50 K, 150 K, and 250 K. During MFCW(T) measurement, the CF90 sample memorizes its locally new equilibrium (low) magnetic states that were generated during field off condition of the MFCC(T) process [9, 15]. The memory effect decreased on decreasing the temperature and negligible at 10 K. On the other hand, MFCC(T) and MFCW(T) curves at 200 Oe without switching off the field at intermediate temperatures (Fig. 3(b)) differed from the magnetic states as shown in Fig. 3(a). The loop formation between MFCC(T) and MFCW(T) curves in Fig. 3(b) shows a thermal cycle induced non-equilibrium magnetic state. It depends on the cooling history, where high magnetic state at the lowest temperature (10 K) is thermally activated to low magnetic state during FCW

mode. The memory effect is noticeably suppressed at cooling field 500 Oe (Fig. 3(c)). Time response of the normalized magnetization ($M(t)/M(t_0)$), recorded during off mode of the cooling fields 200 Oe (Fig. 3(d)) and 500 Oe (Fig. 3(e)), revealed the non-equilibrium spin dynamics. $M(t_0)$ is the first point of $M(t)$ curves recorded waiting time (t_w) at field off condition. The $M(t)$ curves during field off condition of the MFCC(T) process at different temperatures are best fitted with a general function, consisting of a constant term and two exponentially decay terms.

$$M(t) = \alpha_0 \pm \alpha_1 \exp(-t/\tau_1) \pm \alpha_2 \exp(-t/\tau_2) \quad (1)$$

Sign of the pre-factors α_1 and α_2 is taken as positive and negative to represent the magnetization decay and growth, respectively. Out of the two exponential terms, one represents fast relaxation (initial part of the relaxation process) and other one represents a slow relaxation (relaxation process at higher time zone). Similar spin relaxation processes were found in heterogeneous spin structure [27]. The $M(t)$ data at low temperature (50 K) are best fitted with a logarithmic decay function: $M(t) = M_0 - \alpha \ln t$. It represents a slow time response and generally applicable for the systems having a distribution of activation energy [28, 29]. The slope (α) is found to be 0.0002 and 0.0160 (arb. unit) at cooling fields 200 Oe and 500 Oe, respectively. A comparative fit of the $M(t)$ data during OFF condition of 500 Oe at 250 K (Fig. 3(f)) suggest that logarithmic decay satisfied only for a limited portion of the relaxation data, where as the power law equation (1) is widely matched to the $M(t)$ curves. Hence, $M(t)$ data during $M(T)$ and $M(H)$ measurements are fitted with equation (1) having two exponential terms.

We examined the non-equilibrium spin dynamics in the CF90 sample by recording $M(H)$ loop within field ± 70 kOe at 10 K (Fig. 4(a)). The ZFC $M(H)$ loop was recorded at 10 K using protocol PC5. Next, protocol PC6 was applied to record the $M(H)$ curve between +70 kOe to -10 kOe with intermediate waiting at 0 Oe. This process was repeated for 6 times to record the $M(t_w)$

curve at different t_w and the curves are shown in Fig. 4(b). It is seen that $M(H)$ curves between 0 Oe and -10 kOe are extremely sensitive to spin relaxation process during t_w at 0 Oe. The $M(H)$ curves after waiting at 0 Oe moved upward with the increase of t_w with reference to the curve without waiting. On the other hand, $M(t_w)$ curves at 0 Oe (Fig. 4(c)) slowed down at higher t_w and the $M(t_w)$ curves are fitted with equation (1). Fig. 4(d-f) shows waiting time dependence of the fit parameters (H_C , M_0 , α_1 , τ_1 , α_2 , τ_2) from $M(H)$ curves (0 Oe to -10 kOe) and $M(t_w)$ curves at 0 Oe. Coercivity (H_C) of the CF90 sample increased with the increase of t_w at 0 Oe, unlike a decrease of the fit parameter M_0 . The pre-factor α_1 shows an increasing behavior with t_w , unlike a decreasing trend of α_2 . The relaxation time constants (τ_1 , τ_2) both increased with t_w . A wide difference in the magnitude of τ_1 and τ_2 confirms the existence of two relaxation mechanisms.

In Fig. 5(a), we plot $M(H)$ loop of the CF90 sample at 10 K, recorded using conventional FC mode (PC5) at cooling field +70 kOe and -70 kOe. In FC loop (@ +70 kOe), the sample was cooled from 300 K down to 10 K in the presence of +70 kOe and loop was recorded with starting field from +70 kOe to -70 kOe and back to +70 kOe. The FC loops exhibit widening and shifting along field and magnetization directions with improved squareness in comparison to ZFC loop. This indicates that cooling gives preferential rotation of the spins from one locally saturated magnetic state to different magnetic state. The centers (H_{C0} , M_{R0}) and coercivity (H_C) of the FC and ZFC loops have been used to calculate the shift of coercivity ($\Delta H_C = |H_C^{FC} - H_C^{ZFC}|$), exchange bias field ($H_{EB} = H_{C0}^{FC} - H_{C0}^{ZFC}$) and magnetization ($\Delta M_R = M_R^{FC} - M_R^{ZFC}$). As shown in the inset of Fig. 5(a), the FC loop (@ +70 kOe) is nearly symmetric about the center with minor exchange bias shift ($H_{EB} \sim + 8$ Oe) and $H_C \sim 8295$ Oe. The CF90 sample shows a large positive shift of magnetization ($\Delta M_R \sim + 1.55$ emu/g) and coercivity ($\Delta H_C \sim + 1595$ Oe) with respect to ZFC loop with $H_C \sim 6760$ Oe. The FC loop (@ -70 kOe) was recorded during field

sweeping from -70 kOe to +70 kOe and back to -70 kOe. The FC loop (@ -70 kOe) showed similar features, except higher widening ($H_C \sim 8495$ Oe, $\Delta H_C \sim +1735$ Oe, $\Delta M_R \sim +1.99$ emu/g) and squareness in comparison to the FC loop @ +70 kOe. This indicates a fine heterogeneous spin structure with anisotropic response to cooling field directions [13]. It could be an effect of interplay between the exchange and uniaxial anisotropies [8]. After completing the FC loop (@ +70 kOe) measurement at 10 K, the $M(H)$ curve measurement within field range +70 kOe to -10 kOe was repeated for 6 times with intermediate waiting at -2.5 kOe to record the $M(t_w)$ data. Fig. 5(b) demonstrates that magnetic relaxation at -2.5 kOe during waiting time, which varied from 140 s to 7200 s, plays an important role on shaping/designing the upward increase of $M(H)$ curve while recorded in the field range -2.5 kOe to -10 kOe. As shown in Fig. 5(c), the $M(t_w)$ curves at -2.5 kOe are well fitted with equation (1). In addition to a significant increase of the coercivity (Fig. 5(d)-left Y axis), the overall magnetization after -2.5 kOe and the fit parameter M_0 (Fig. 5(d)-right Y axis) have been increased with the increase of t_w . The fit parameter α_2 decreased, unlike an increasing tendency of α_1 with t_w (Fig. 5(e)). On the other hand, time constants τ_1 (fast relaxation) and τ_2 (slow relaxation) both increased with t_w , although magnitude of τ_2 is at higher side (Fig. 5(f)).

We also tested non-equilibrium spin dynamics of the CF90 sample at 150 K, which is just above the magnetization blocking temperature at about 125 K in the MZFC(T) curve for applied magnetic field 50 kOe (top-right axes of Fig. 6(a)). The magnetic domain wall pinning is less effective at this temperature. The $M(H)$ curve, after zero field cooling, was measured at 150 K with field variation from +70 kOe to -6 kOe with an intermediate waiting at -1 kOe (bottom-left axes of Fig. 6(a)). After measurement of the first $M(H)$ curve, the field was made to zero and back to +70 kOe before starting the next curve and repeated it for 7 times. Fig. 6(b) represents

the relaxation regime of $M(H)$ curves at -1 kOe during waiting time and field dependent regime during field sweeping (- 1 kOe to -5 kOe). Fig. 6(c) shows that magnitude of the $M(H)$ curves after waiting at field -1 kOe is suppressed, unlike an increasing increment for similar experiment at 10 K (Fig. 4(b)). The $M(t_w)$ curves also followed equation (1) in the relaxation regime (inset of Fig. 6(c)). The fit parameters are shown in Fig. 6(d-f). The coercivity showed a small increment with the increase of t_w (Fig. 6(d)), whereas the fit parameter M_0 decreases with the increase of t_w . The pre-exponential factors and time constants increased with waiting time. The fit parameters (α_1, τ_1) associated with fast relaxation process are significantly less in values than the parameters associated with slow relaxation process (α_2, τ_2). Although α_2 are saturated at higher waiting time, but the pre-factor α_1 continues to increase with t_w .

3.2 Temperature and field dependent magnetization [$M(T, H, t_w)$] for CF80_BTO sample

The MZFC(T) and MFC(T) curves of the composite sample at 500 Oe (Fig. 7(a)) showed blocking temperature (T_m) of the magnetic domains at about 300 K and wide bifurcation at low temperatures. In addition to a bifurcation between MZFC and MFC curves, the basic magnetic features of the ferrite particles, e.g., a weak temperature dependent MZFC regime below 150 K, are retained in BTO matrix. The temperature dependence of MZFC curves at different magnetic fields up to 50 kOe has shown an increasing magnitude of MZFC(T) curves and shift of the MZFC(T) peak to lower temperatures (Fig. 7(b)). First order derivative of the MZFC(T) curves ($\partial MZFC/\partial T$) at different magnetic fields (Fig. 7(c)) showed an asymmetric shape on both sides of the peak temperature (T_p). The distribution of magnetic interaction/anisotropy in the material has been realized by fitting the asymmetric peak profile with Lorentzian curve. The peak width represents the distribution of anisotropy barriers. It is noted that peak height of the $\partial MZFC/\partial T$ curves initially increased for field up to 2.5 kOe, followed a gradual decrease at higher fields.

This corresponds to a minimum peak width at 2.5 kOe (Fig. 7(d)), along with an increase of peak width both at lower and higher magnetic fields. An increase of the peak height and decrease of width at initial stage of the field increment reveals magnetic field induced nucleation of domains by de-pinning the spins at domain walls. The increase of broadness with reduced peak height for fields higher than 2.5 kOe is attributed to an increase of intrinsic disorder, arising from a competition of the anisotropy constants and exchange interactions inside or at the interfaces of the domains or grain boundaries of the composite material.

The memory effect was studied using PC4 at cooling field 200 Oe, 500 Oe, 1 kOe, 5 kOe, 10 kOe (Fig. 8(a-d)). The cooling field was intermediately switching off during MFCC(T) measurement at 250 K, 150 K, 50 K for 1600 s for recording the off-field $M(t_w)$ data. After completing the MFCC(T) measurement down to 10 K, MFCW(T) data was recorded while temperature was increasing up to 300 K without putting OFF the magnetic field. The MFCW(T) curves shows a local magnetization dip at the temperatures where field was switched off during FCC mode. The CF80_BTO sample also showed reduction of memory effect on lowering the temperature and increase of the magnetic fields. The % drop of magnetization and relaxation of magnetization during field off condition with respect to the in-field MFC(T) magnetization have been compared for the samples CF90 and CF80_BTO in Fig. 8(e) and Fig. 8(f), respectively. There are some distinct differences in the composite sample. The drop of magnetization before relaxation with respect to MFCC(T) magnetization is significantly high than the relaxation of magnetization during waiting time, as schematized in the inset of Fig. 8(e). The drop of off-field magnetization for cooling field (H_{FC}) 500 Oe is found to be less than the magnetic reduction for $H_{FC} = 200$ Oe in case of CF90 sample, whereas the composite sample has shown a monotonic increase of the magnetic drop with the increase of H_{FC} up to 10 kOe. The higher magnetic

reduction in composite sample during field off condition indicates weak magnetic interactions at the interfaces of CFO (ferrimagnetic) and BTO (non-magnetic) particles [10]. As shown in Fig. 9 (a-d), normalized $M(t_w)$ curves of the composite sample during field off condition are fitted with equation (1). The magnetization values ($M(0)$) used for normalization are plotted in Fig. 9 (e) and the behavior is expected with the variation of magnetic field and temperature. The fit parameters (time constants τ_1 and τ_2 , pre-factors α_1 and α_2) are shown in of Fig. 9(f-i). These parameters are less sensitive to higher magnetic fields (5 kOe and 10 kOe). However, the τ_1 value at different H_{FC} has increased on decreasing the temperature by complementing a decrease of the values of τ_2 . However, both the pre-factors (α_1 and α_2) decreased with the decrease of measurement temperature.

The in-field magnetic relaxation was studied at temperatures 10 K, 50 K, 100 K, 150 K, 200 K, 250 K and 300 K after zero field cooling of the composite sample from 330 K. A constant magnetic field (say, 500 Oe) was applied after temperature stabilization at 10 K. The sample was waited for 100 s before recording the in-field $M(t)$ data for 3600 s. After completing the $M(t)$ measurement at 10 K, the field was made off by oscillatory mode and the sample was warmed up (@3 K/min) to the next temperature 50 K, where the sample was waited for 10 minutes before recording the in-field $M(t)$ data using the same procedure as adopted at 10 K. The in-field $M(t)$ data were recorded at other temperatures up to 300 K. Similar procedure was followed to record the in-field $M(t)$ data in the presence of fields 1 kOe, 5 kOe, 10 kOe and 20 kOe. Fig. 10(a-e) shows the in-field $M(t)$ data (normalized) at different temperatures (marked in Fig. 10(a)). The in-field magnetization increased with time. The $M(0)$ values (Fig.10(f)), used to normalize $M(t)$ data, is consistent to the variation of magnetic fields at different temperatures in Fig. 7(b). The in-field $M(t)$ data are scattered at temperatures above 200 K and also at higher magnetic field 20

kOe. This is related to increasing number of non-blocking spins at higher temperatures. The non-blocking regime of magnetization extends to lower temperatures by increasing the applied field. The in-field $M(t)$ curves obeyed equation (1) with two time constants (τ_1, τ_2) and two pre-factors ($-\alpha_1, -\alpha_2$). The fit parameters are shown in Fig. 11 (a-d). The time constants are relatively large at low temperatures, where spin dynamics is slow due to strong anisotropy/domain wall pinning. The negative value of pre-factors takes into account the in-field magnetization growth with time. The relaxation rate is maximum at a temperature close to the onset of non-blocking regime of the MZFC(T) curves depending on applied fields, e.g., at 150 K for low magnetic fields (500 Oe and 1 kOe) and at 10 K for higher magnetic fields.

We also measured zero field cooled $M(H)$ loop of the composite sample at 10 K with the field sequence +70 kOe to 0 Oe and $M(t_w)$ curve measurement at 0 Oe (P1) during waiting time for 1 hr. This is followed by resumption of the $M(H)$ measurement down to -7 kOe (P2), where the sample was waited for 1 hr to record the second $M(t_w)$ curve. Then, recording of $M(H)$ curve was continued down to field at -70 kOe. The field was reversed back to +7 kOe (P3) where third $M(t_w)$ data were recorded for 1 hr. Finally, $M(H)$ curve was recorded by increasing the field up to +20 kOe. A similar $M(H)$ measurement protocols were used to record the $M(t_w)$ curves at 10 K after cooling the sample in the presence of +70 kOe from 300 K. The same experiments after ZFC and FC of the sample were carried out at 100 K. Fig. 12 (a-b) shows the recorded ZFC and FC $M(H)$ curves. It is interesting to note that non-equilibrium $M(t_w)$ data at point P2 and P3 started to relax towards the zero magnetization state in the presence of waiting field at + 7 kOe (+4 kOe) and - 7 kOe (-4 kOe), respectively. The behavior is consistent to the simulated results for the polycrystalline exchange-bias bilayered systems [30], where the spins ordered along a particular direction at high fields will experience a torque when the field is reduced to zero and

rotate the over a time toward the positive or negative direction, depending on the local easy-axis orientation. The FC loop at 10 K shows nearly symmetric widening along the field and magnetization axes. The widening is extremely small at 100 K. The (normalized) $M(t_w)$ curves, as shown in Fig. 12(c-d), exponentially decayed with two time constants. The $M(0)$ values are positive and negative for points P2 and P3, respectively. The $M(t_w)$ curves after ZFC and FC processes showed no differences at 10 K and 100 K for field-in wait at 0 Oe. The normalized $M(t_w)$ curves after FC process significantly enhanced for field in-wait ± 7 kOe at 10 K and ± 4 kOe at 100 K in comparison to the curves after ZFC process. The differences between $M(t_w)$ curves measured after FC and ZFC processes substantially decreased at 100 K. The $M(t_w)$ curves in positive field side (+7 kOe at 10 K and + 4 kOe at 100 K) are also found to be higher than their counter parts in the negative field side. This indicates non-uniform unidirectional anisotropy under cooling field directions [30]. Fig. 10(e-f) shows the time constants (τ_1 , τ_2) at different fields in-wait in FC process are larger than that in ZFC process both at 10 K and 100 K. This indicates slowing down of the relaxation process after field cooling due to additional spin order in the system. However, the τ_1 showed higher values at 100 K than the values at 10 K. This is in contrast to the higher τ_2 values at 10 K than that at 100 K.

The field in-waiting time effect on the exchange bias effect or variation of the coercivity in the composite sample has been investigated by measurement of ZFC and FC $M(H)$ curves at 10 K (Fig. 13 (a)) and 150 K (Fig. 13(b)). In this experiment, the sample was first zero field cooled from 300 K to 10 K/150 K and $M(H)$ curve ($N = 1$) was measured during sweeping of the field from +70 kOe to -20 kOe (10 K) or complete loop was measured at 150 K. After first round measurement, the applied field was made zero before increasing the temperature to 300 K. Next, the sample was cooled under +70 kOe down to 10 K/150 K. After temperature stabilization, the

$M(H)$ curve ($N = 2$) was recorded from +70 kOe to -20 kOe with an intermediate waiting at - 7 kOe for 10 K and at -2150 Oe for 150 K. The in-field $M(t_w)$ curve was recorded during waiting time. The FC- $M(H)$ curve in the field range +70 kOe to -20 kOe with intermediate waiting were repeated for different t_w and normalized $M(t_w)$ curves are shown for 10 K (Fig. 13(c)). The changes in FC- $M(H)$ curves at -2150 Oe during waiting time at 150 K are shown in Fig. 13(d). As plotted in the inset of Fig. 13(a), H_C of the FC curves at 10 K is higher than that in ZFC curve. Also, H_C in FC loop depends on waiting time at - 7 kOe. On the other hand, in-field (at - 2150 Oe) magnetic relaxation of the FC curve at 150 K is very fast. The magnetization switches from positive to negative by increasing the waiting time greater than 180 s, although H_C of the ZFC curve (-2533 Oe) is larger than the wait-in field H_C value (-2150 Oe). The decrease of H_C in FC curves at 150 K with the increase of waiting time at -2150 Oe is opposite in character with respect to the increment of H_C with field-in waiting time at 10 K. The t_w at 10 K was made high enough to observe an appreciable relaxation, indicating a strong anisotropy/domain wall pinning. The in-field $M(t_w)$ curves at 10 K fitted with logarithmic decay law $M(t_w) = \alpha_0 - m \cdot \ln t_w$ (Fig. 13(c)). The inset of Fig. 13(c) shows the decrease of both α_0 and slope (m) with the increase of waiting time at - 7 kOe of the FC- $M(H)$ curves. In contrast, the in-field $M(t_w)$ curves at 150 K fitted with exponential law (1). The fitted parameters are not shown in the plot. Finally, we tested the effect of field sweeping rate during measurement of the $M(H)$ curves of the composite sample from +70 kOe to -15 kOe at 10 K (Fig. 14(a)) and +70 kOe to -1 kOe at 300 K (Fig. 14(b)). In this experiment at 10 K (300 K), the sample was zero field cooled from 300 K (330 K) and measurement of the $M(H)$ curve was repeated for different sweeping rate of field without further heating to higher temperature. The $M(H)$ curves at 10 K are practically independent of the field sweeping rate, whereas the $M(H)$ curves at 300 K showed a relaxation/fatigue effect.

4. Summary and conclusions

In the ferrite sample (CF90), we assume multi-domain structured ferrimagnetic particles. Inside each particle, the domains are separated by domain-walls. The spins inside each domain are ferrimagnetically ($\uparrow\downarrow\uparrow\downarrow$) ordered and disordered or pinned at the domain-walls. Further, each magnetic particle is assumed to be core-shell configuration [12, 18]. The core (interior) part is consisting of more than one domain and associated domain-walls. The shell (outer) part spreads over few lattice parameters whose length is more than domain-wall thickness and its spins are more disordered than that inside the core. The magnetic exchange interactions inside the core are stronger than the exchange interactions at shell. Hence, there will be three sources of spins to respond, viz., domain, domain-wall and shell, under the application or switching-off of external magnetic field. In case of the composite material, magnetic exchange interactions at the interfaces are diluted. This is evidenced from the increase of ferrimagnetic softness in composite sample. There is a possibility of magneto-electric coupling at the interfaces of CF80 and BTO particles [16-17] or a hidden interface driven exchange coupling in oxide heterostructures [31]. Temporal evolution of the local spins is expressed by Landau-Lifshitz-Gilbert equation, $\frac{d\vec{M}}{dt} = -\gamma_0(\vec{M} \times \vec{H}_{\text{eff}}) + \frac{\alpha}{M_S}(\vec{M} \times \frac{\partial \vec{M}}{\partial t})$, where γ_0 is the gyromagnetic ratio and α is the Gilbert damping factor [32]. The equation can be re-written as $\frac{d\vec{M}}{dt} = -\gamma_0(\vec{M} \times \vec{H}_{\text{ext}}) + \frac{\alpha}{M_S}(\vec{M} \times \frac{\partial \vec{M}_{\text{eff}}}{\partial t})$, where $\frac{\partial \vec{M}_{\text{eff}}}{\partial t} = \frac{M_S}{\alpha} \vec{H}_{\text{int}} + \frac{\partial \vec{M}}{\partial t}$ [33]. A competition between the free spin torque under external field (first term) and damping torque (second term) under internal field determines the relaxation/orientation of spin vectors towards its nearest low energy magnetic state. We assume that the spin relaxation due to damping term includes the combined effects of the magnetic exchange

coupling between interfaces of core (FiM) and shell (disordered FiM), shell (disordered FiM) and shell (disordered FiM), and shell (disordered FiM) and shell (non-magnetic and ferroelectric-BTO). The heterogeneous spin structure in the systems plays a vital role in tuning the non-equilibrium spin dynamics (memory effect, training effect, exchange bias, coercivity and magnetization) [3-4, 9-10, 13]. The heterogeneous spin structure with the core of FM-Co and shell of AFM-CoO produced a large exchange bias shift when the system was field cooled from a temperature higher than the Neel temperature of AFM-CoO [34]. A thermal activation model has been proposed to understand different forms of the exchange bias effect [35]. The AFM grains are considered to be exchange decoupled while neighboring FM-FM and FM-AFM grains are strongly exchange coupled. The coherent reversal of the decoupled AFM spins is governed by thermally activated processes. The field cooled hysteresis loop gets displaced when AFM spins are rigidly bound to the lattice. The material shows a symmetric hysteresis loop shift when AFM spins are loosely bound to the lattice, although the material can exhibit a non-vanishing rotational hysteresis if exchange anisotropy of the FM-AFM interfacial coupling is greater than the magneto-crystalline anisotropy of the AFM spin-lattice coupling [6]. The training effect is observed when the AFM spins approach to equilibrium magnetic states after subsequent cycling of the hysteresis loop. In most of the systems with training effect, the coercivity and exchange bias field has decreased [8, 13, 35]. However, change of the coercivity in our system is strongly dependent on the regime below magnetic blocking temperature (≥ 300 K). The coercivity has increased at low temperature (10 K) and decreased at higher temperature (150 K) on repeating the M(H) measurement. The tuning of coercivity and magnetic state by employing various protocols for recording off-field and in-field time dependent measurement of magnetization on

the temperature and field dependent magnetization curves could provide a better opportunity for designing multi-state magnetic switch, magnetic sensor and magnetic recording devices [36-38].

We conclude that ferrimagnetic $\text{Co}_{1.75}\text{Fe}_{1.25}\text{O}_4$ (CF90 sample) and its composite with non-magnetic BaTiO_3 (CF80_BTO sample) exhibited ferrimagnetic properties for temperatures up to 300 K (room temperature) and above. In case of the composite material, the interfacial/shell parts of the two particles in contact are strongly modified by the presence of non-magnetic and ferroelectric BTO particles. The existence of intrinsic disorder inside the magnetic domains is confirmed by magnetic memory and magnetic relaxation effects. The systems exhibited magnetic memory effect at relatively higher temperatures and exchange bias effect at lower temperatures. The absence of asymmetric hysteresis loop at low temperature after field cooling the samples indicates a strong magnetic exchange coupling between ferrimagnetic particles. The time relaxation of magnetization has been used as a powerful technique to get insight of the non-equilibrium spin switching process during field off or field-in conditions of the temperature and field dependence of magnetization measurements. Experimental results confirm the existence of two relaxation mechanisms; a fast relaxation with time constant τ_1 and a slow relaxation with time constant τ_2 . The fast relaxation process (dominated at the initial stage of the relaxation) arises most probably from the loosely bound shell/interfacial spins, whereas the slow relaxation process (dominated at the later stage of the relaxation) contributes most probably from strongly interacting core/interior spins in the systems. The training effect is not much prominent in our systems, but magnetic state and coercivity are strongly dependent on the in-field or off-field waiting time during $M(H)$ measurements. The $M(H)$ curves at low temperatures (strong anisotropic regime) are practically independent of the field sweeping rate, where as $M(H)$ curves at 300 K (non-blocking magnetic regime) showed a minor relaxation at higher field side.

Acknowledgment

RNB acknowledges the research support from BRNS (Grant No. 2011/37P/45/BRNS/2628) and UGC (F. No. F.42-804/2013 (SR)), Government of India for carrying out this research work.

References

- [1] D.S. Mathew, and R.-S. Juang, *Chemical Engineering Journal* **129**, 51 (2007).
- [2] A. Walsh, Su-H. Wei, Y. Yan, M.M. Al-Jassim, and J.A. Turner, *Phys. Rev. B* **76**, 165119 (2007).
- [3] J. Nogues, J. Sort, V. Langlais, V. Skumryev, S. Surinach, J.S. Munoz, and M. D. Baro, *Phys. Rep.* **422**, 65 (2005).
- [4] J. Nogues, and I. K. Schuller, *J. Magn. Magn. Mater.* **192**, 203 (1999).
- [5] R.N. Bhowmik, V. Vasanthi, A. Poddar, *J. Alloys Compd.* **578**, 585 (2013).
- [6] W. H. Meiklejohn, *J. Appl. Phys.* **33**, 1328 (1962).
- [7] S. Polisetty, S. Sahoo, A. Berger, and Ch. Binek, *Phys. Rev. B* **78**, 184426 (2008).
- [8] R. Wu, J. B. Fu, D. Zhou, S. L. Ding, J. Z. Wei, Y. Zhang, H. L. Du, C. S. Wang, Y. C. Yang, and J. B. Yang, *J. Phys. D: Appl. Phys.* **48**, 275002 (2015).
- [9] J. Carrey, B. Mehdaoui, and M. Respaud *J. Appl. Phys.* **109**, 083921 (2011).
- [10] R. Malik, N. Sehdev, S. Lamba, P. Sharma, A. Makino, and S. Annapoorni, *Appl. Phys. Lett.* **104**, 122407 (2014)
- [11] J. Barman, T. Bora, S. Ravi, *J. Magn. Magn. Mater.* **385**, 93 (2015).
- [12] K. Nadeem, H. Krenn, D.V. Szabó, *J. Magn. Magn. Mater.* **393**, 239 (2015).
- [13] P.K. Manna, and S.M. Yusuf, *Phys. Reports* **535**, 61 (2014).
- [14] Y. Zhang, Z. Yang, B.-P. Zhu, J. Ou-Yang, R. Xiong, X.-F. Yang, and S. Chen, *J. Alloys Compd.* **514**, 25 (2012).

- [15] Z. Tian, L. Xu, Y. Gao, S. Yuan, Z. Xia, *Appl. Phys. Lett.* **111**, 182406 (2017).
- [16] C. Sen, W.A.S Aldulaimi, O. Mohammadmoradi, and I.B. Misirlioglu, *J. Phys. D: Appl. Phys.* **52**, 015305 (2019).
- [17] T. Vimal, S. Pandey, S.K. Gupta, D.P. Singh, K. Agrahari, G. Pathak, S. Kumar, P.K. Tripathi, R. Manohar, *Liquid Crystals* **45**, 687 (2018).
- [18] G. J. Kumar, C. Rath, *J. Magn. Magn. Mater.* **466**, 69(2018)
- [19] K. Inomata, N. Ikeda, N. Tezuka, R. Goto, S. Sugimoto, M. Wojcik, and E. Jedryka, *Sci. Technol. Adv. Mater.* **9**, 014101 (2008).
- [20] S. Hoffman, Y. Tserkovnyak, P.K. Amiri, and K.L. Wang, *Appl. Phys. Lett.* **100**, 212406 (2012)
- [21] R.N. Bhowmik, S. Kazhugasalamoorthy, R. Ranganathan, and A.K. Sinha, *J. Alloys Compd.* **680**, 315 (2016).
- [22] R.N. Bhowmik, S. Kazhugasalamoorthy, and A.K. Sinha, *J. Magn. Magn. Mater.* **444**, 451 (2017).
- [23] H. L. Trong, L. Presmanes, E. D. Grave, A. Barnabe, C. Bonningue, Ph. Tailhades, *J. Magn. Magn. Mater.* **334**, 66 (2013).
- [24] R.N. Bhowmik, M.R. Panda, S.M. Yusuf, M.D. Mukadam, A.K. Sinha, *J. Alloys Compd.* **646**, 161 (2015).
- [25] J.A. González, J.P. Andrés, R. L. Antón, J. De Toro, P.S. Normile, P. Muñoz, J. M. Riveiro, and J. Nogués, *Chem. Mater.* **29**, 5200 (2017).
- [26] G. Catalan, J. Seidel, R. Ramesh, and J.F. Scott, *Rev. Modern. Phys.* **84**, 119 (2012).
- [27] Y. Takagaki, J. Herfort, L. Däweritz, and K. H. Ploog, *Phys. Rev. B* **74**, 224417 (2006).
- [28] R.N. Bhowmik, and R. Ranganathan, *J. Magn. Magn. Mater.* **237**, 27 (2001).

- [29] R.V. Chamberlin, K.D. Humfeld, D. Farrell, S. Yamamuro, Y. Ijiri, and S.A. Majetich, J. Appl. Phys. **91**, 6961 (2002).
- [30] M. D. Stiles, and R. D. McMichael, Phys. Rev. B **63**, 064405 (2001).
- [31] A. Chen et al., Adv. Mater. **29**, 1700672 (2017).
- [31] V. Skumryev, V. Laukhin, I. Fina, X. Martí, F. Sa´nchez, M. Gospodinov, and J. Fontcuberta, Phys. Rev. Lett. **106**, 057206 (2011).
- [32] R.N. Bhowmik, and A.G. Lone, J. Magn. Magn. Mater. **462**, 105 (2018).
- [33] T. R. Gao, Z. Shi, S. M. Zhou, R. Chantrell, P. Asselin, X. J. Bai, J. Du, and Z. Z. Zhang, J. Appl. Phys. **105**, 053913 (2009).
- [34] R. Skomski, J. Phys.: Condens. Matter **15**, R841 (2003).
- [35] V. Kumari, K. Dey, S. Giri, and A. Bhaumik, RSC Adv. **6**, 45701 (2016).
- [36] W. H. Meiklejohn and C. P. Bean, Phys. Rev. **102**, 1413 (1956).
- [37] S. Giri, M. Patra, and S. Majumdar, J. Phys.: Condens. Matter **23**, 073201 (2011).

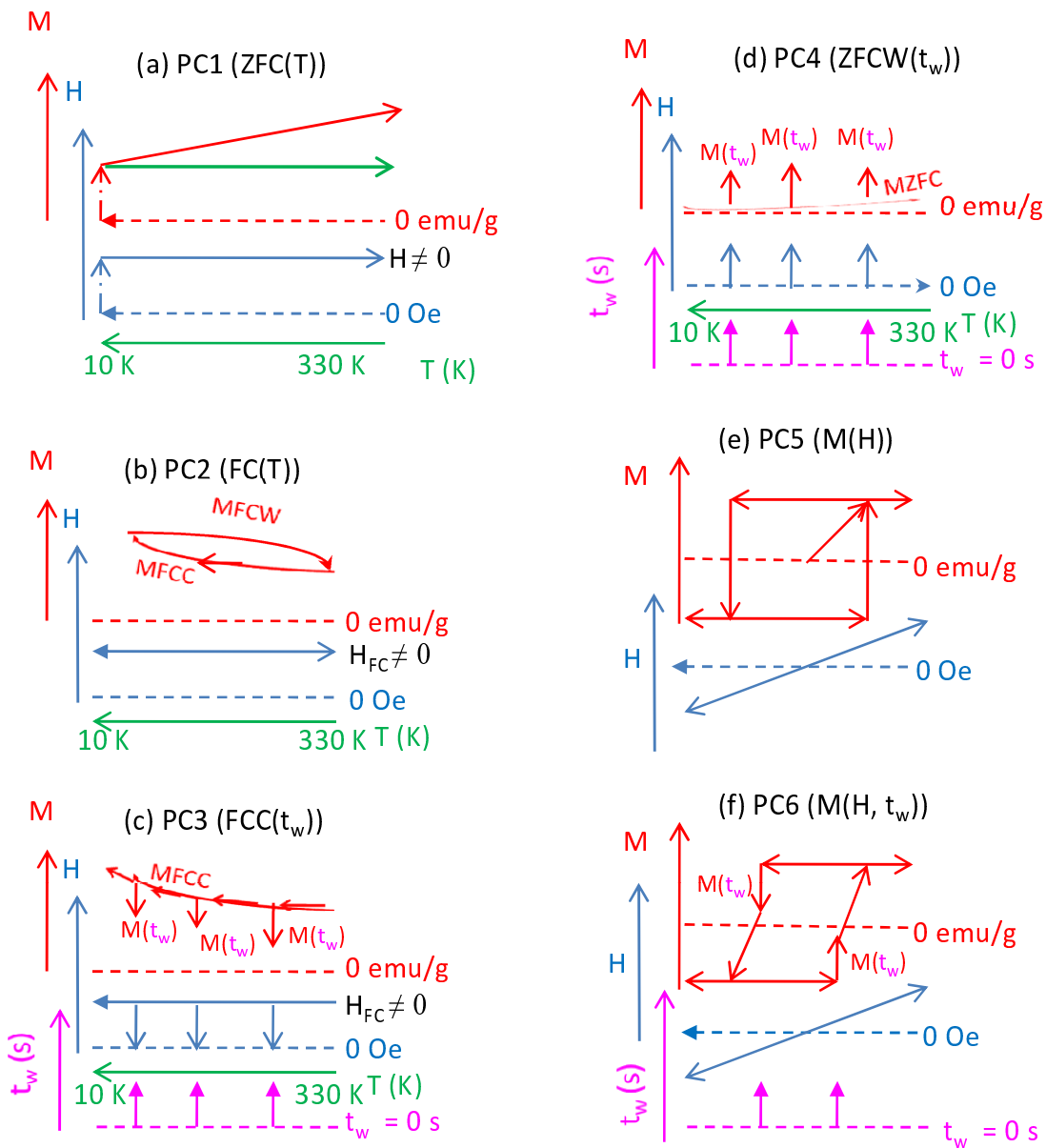


Fig. 1 Measurements of the temperature dependence of magnetization (a-d) and the field dependence of magnetization (e-f), where new protocols were incorporated for recording the time response of the magnetization. At selected temperatures, the cooling field was made off during MFCC(T) mode of measurement (c) and the field was made ON during MZFCW(T) mode of measurement for waiting time t_w to record the $M(t_w)$ data. In comparison to conventional M(H) loop (e), the M(H) measurement was waited at selected fields just before coercive field points on the positive and negative field axes for waiting time t_w to record the $M(t_w)$ data (f).

CF90 sample

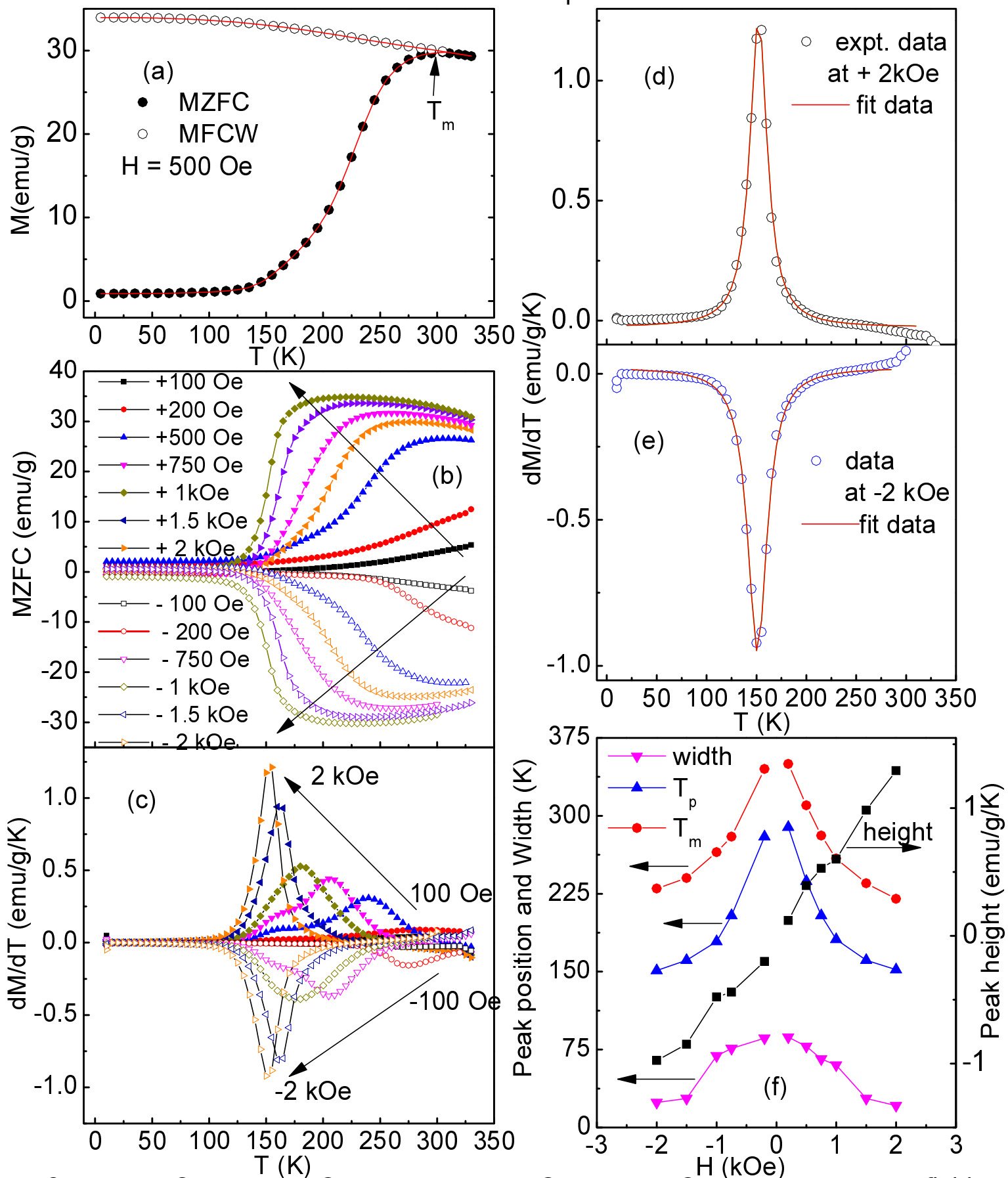


Fig. 2 The MZFC(T) and MFCW(T) data at 500 Oe (a), MZFC(T) data at selected fields (b), first order derivative of the MZFC(T) data in (b), i.e., dM/dT curves (c), fit of the dM/dT curves at +2 kOe (d) and at -2 kOe (e). The peak parameters at different fields (f).

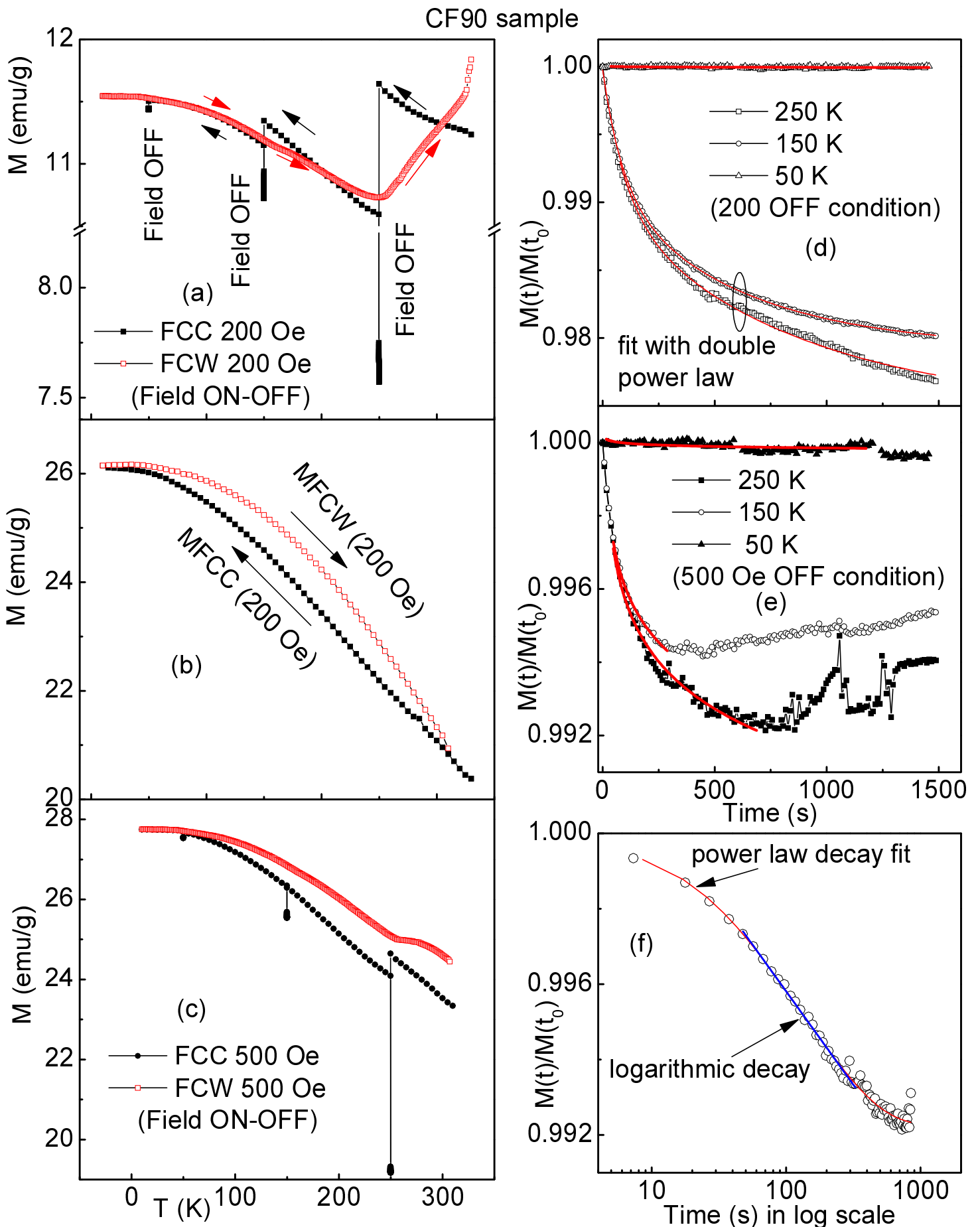


Fig. 3 MFCC(T) with intermediate field OFF and MFCW(T) at 200 Oe (a). MFCC(T) and MFCW(T) curves at constant 200 Oe (b). $M(t)$ data (normalized) at three temperatures during field off at 200 Oe (d and 500 Oe (e). A comparative fit of $M(t)$ data at 250 K (f).

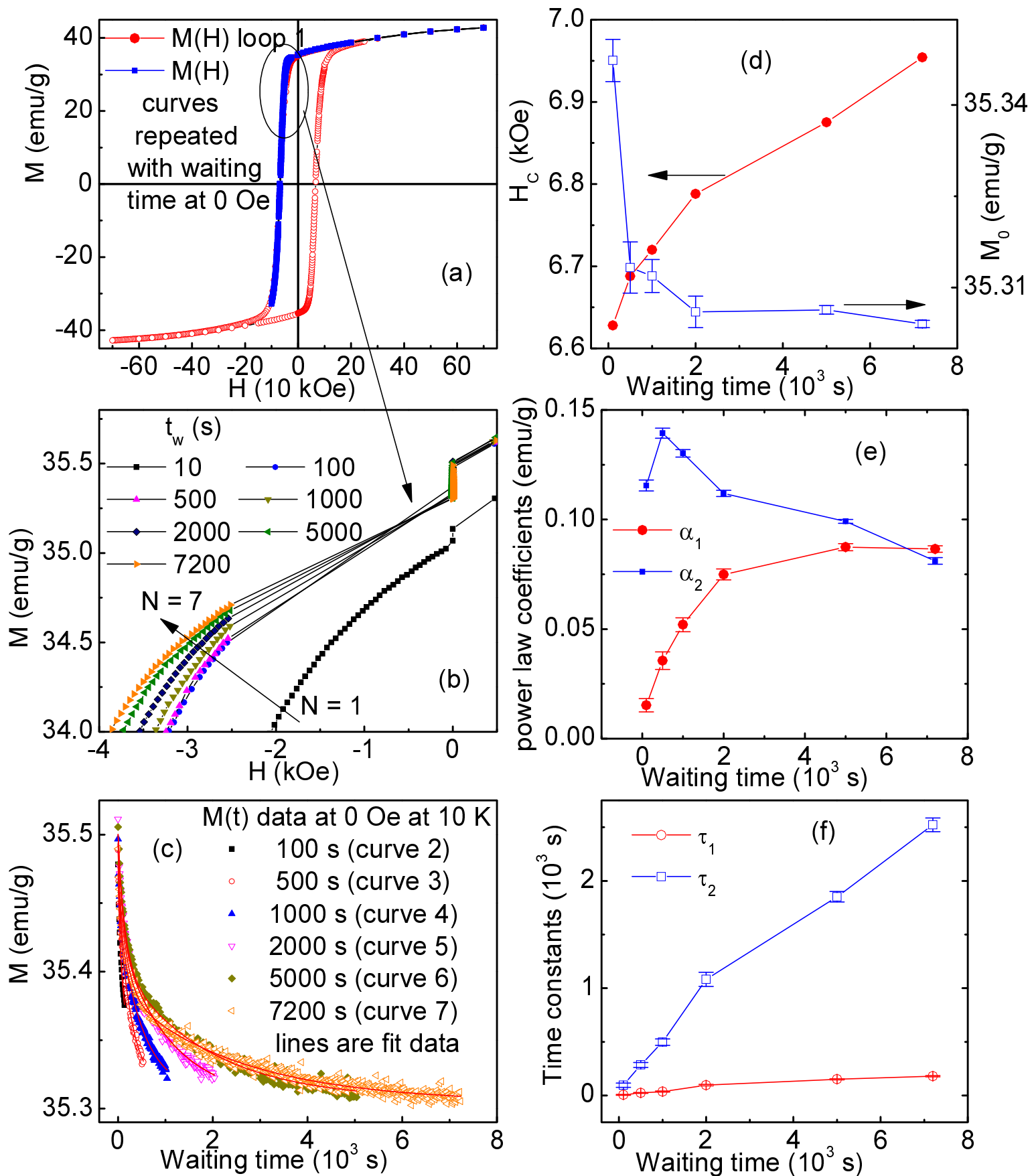


Fig. 4 $M(H)$ loop within ± 70 kOe and repetition of $M(H)$ curves from $+70$ kOe to -15 kOe with recording of magnetization for different waiting time at 0 Oe (a). Variation of $M(H)$ curves after waiting time (b). $M(t)$ data during waiting time, along with fit data (c). Waiting time dependence of coercivity and initial magnetization (d) and fit parameters of CF90 sample at 10 K (e-f).

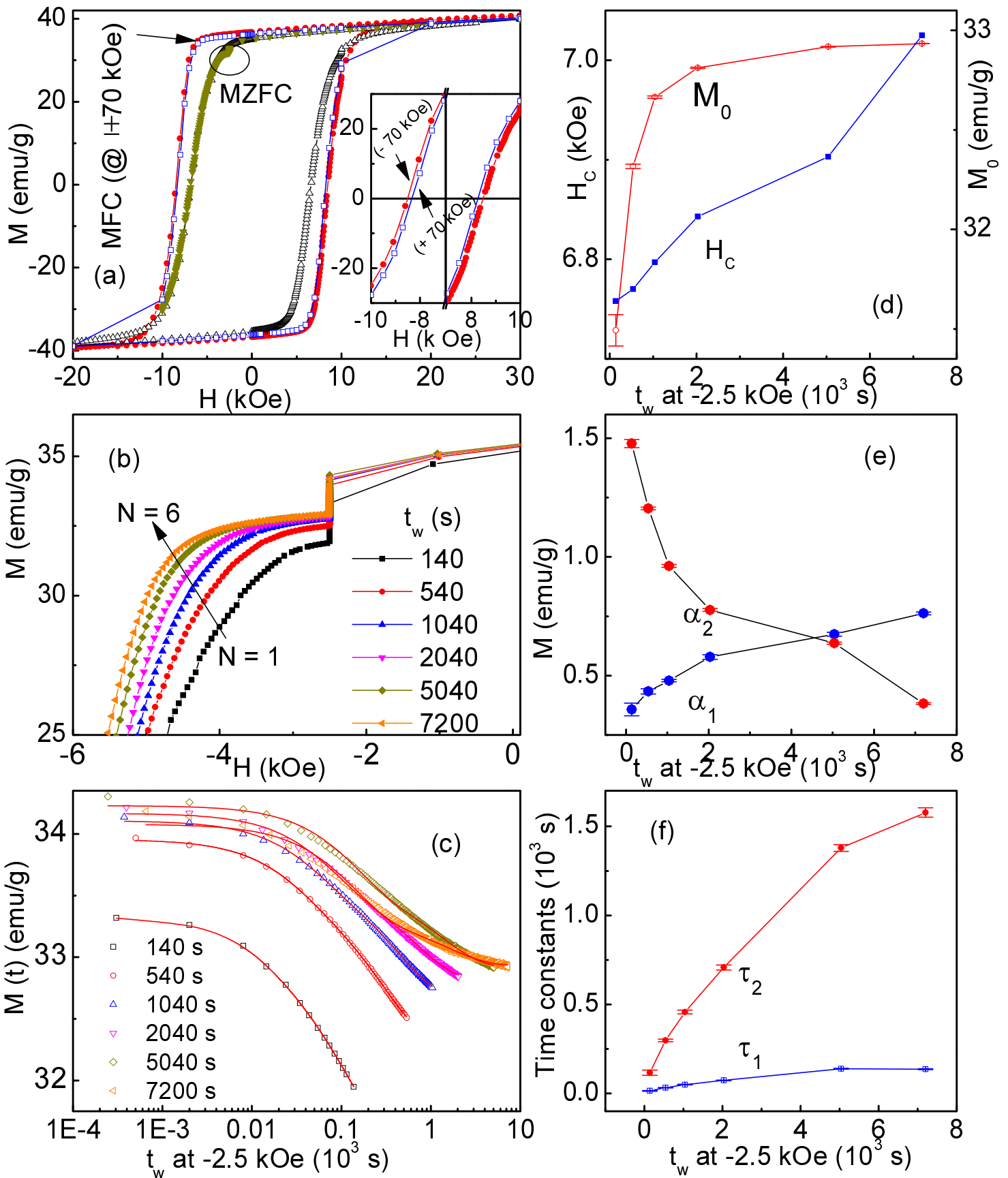


Fig. 5 (a) The $M(H)$ loop in ZFC and FC @ ± 70 kOe modes at 10 K and inset shows the difference in FC loop under $+70$ kOe and -70 kOe. The $M(H)$ curve in ZFC mode was repeated with different waiting time at -2.5 kOe and the effect is shown in (b). The fit of $M(t)$ data during waiting time (c) and the variation of fit parameters are shown in (d-f).

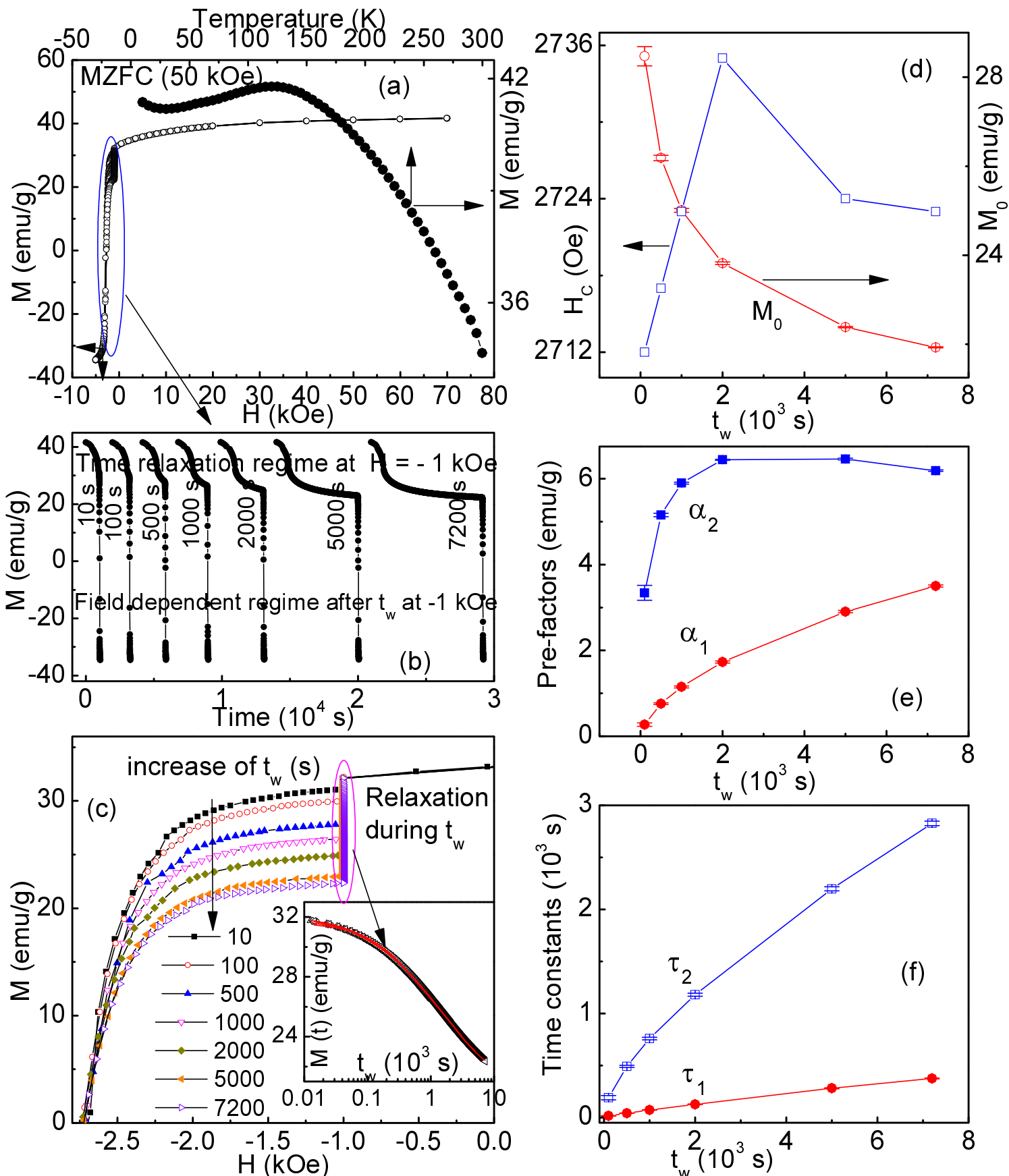


Fig. 6 (a) $M(H)$ curves of CF90 sample have been repeated with different waiting time at -1 kOe at the measurement temperature 150 K (bottom-left axis), which is near to top of the MZFC(T) curve measured at 50 kOe (top-right axis). The time relaxation and field dependence regime of magnetization (b). The $M(H)$ curve is affected by the t_w at -1 kOe (c). Fit of the $M(t)$ data using exponential law (inset of c) and fit parameters (d-f).

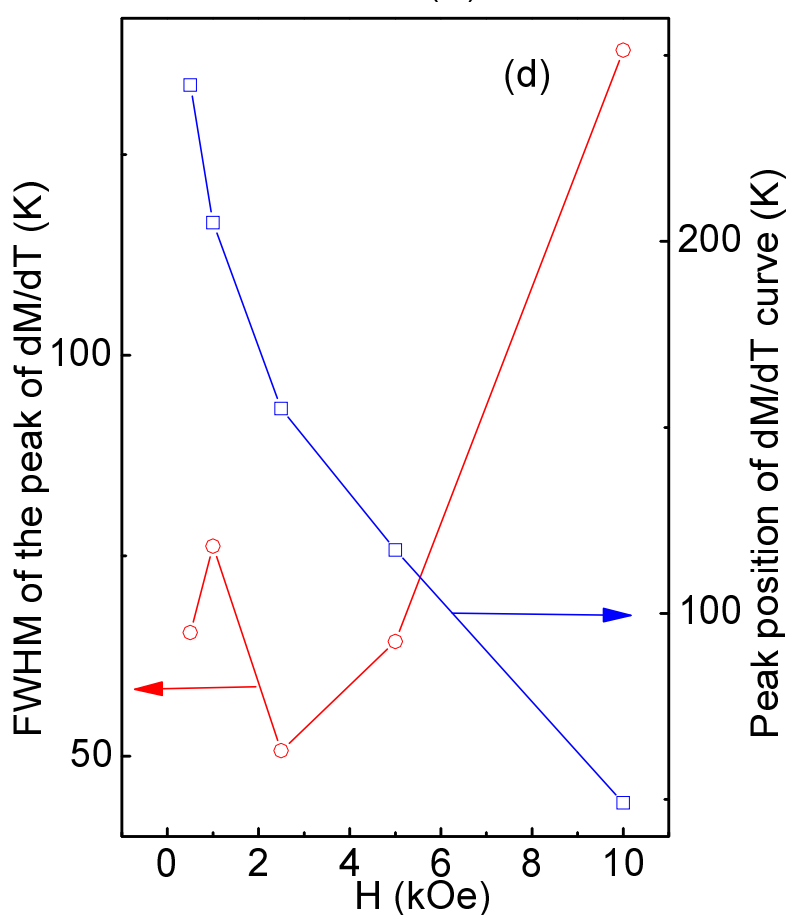
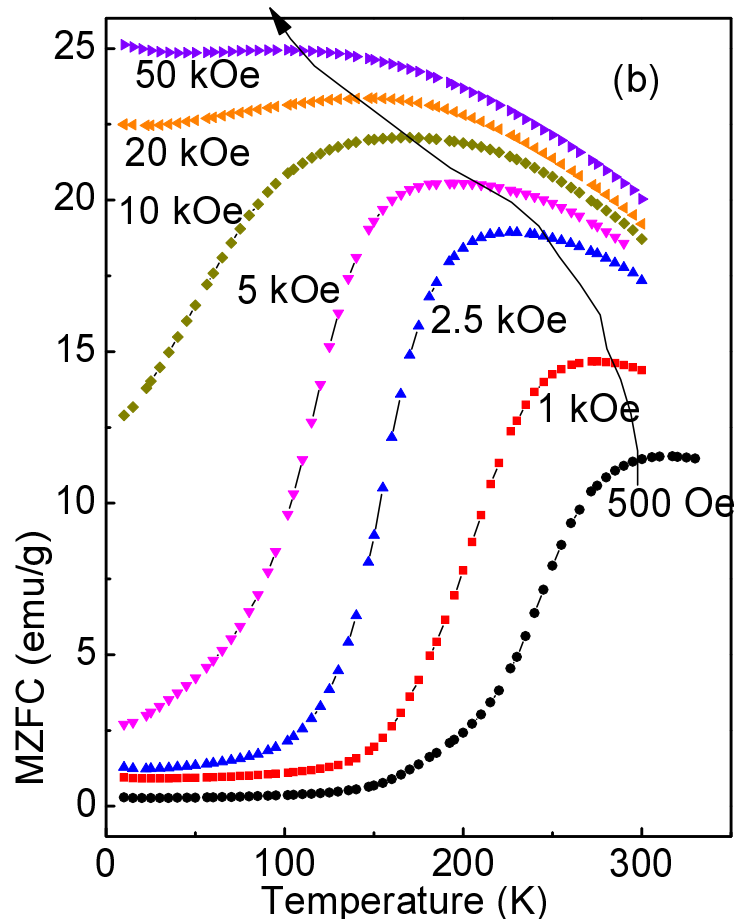
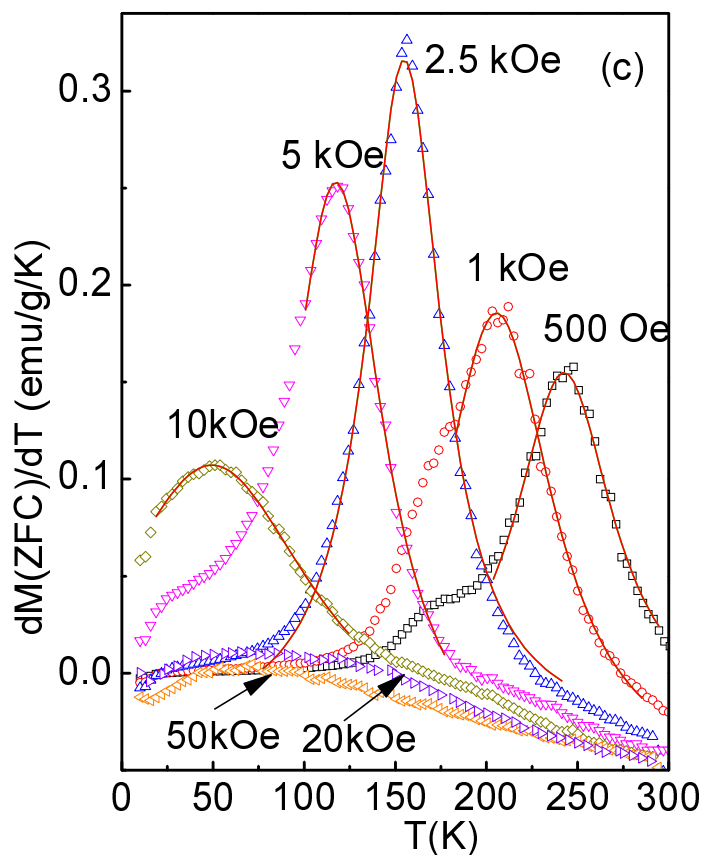
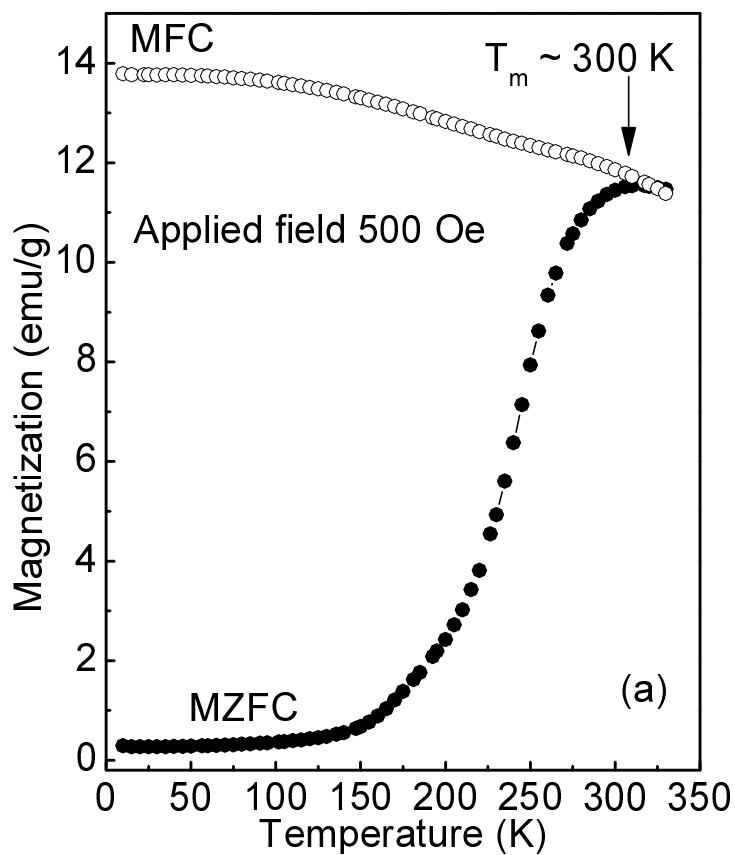


Fig. 7 MZFC(T) and MFC(T) curves at 500 Oe (a). The MZFC (T) curves at different applied fields (b). The temperature derivative of MZFC curves (in b) along with fit of the peaks with Lorentzian shape (c) and variation of the peak parameters with field (d).

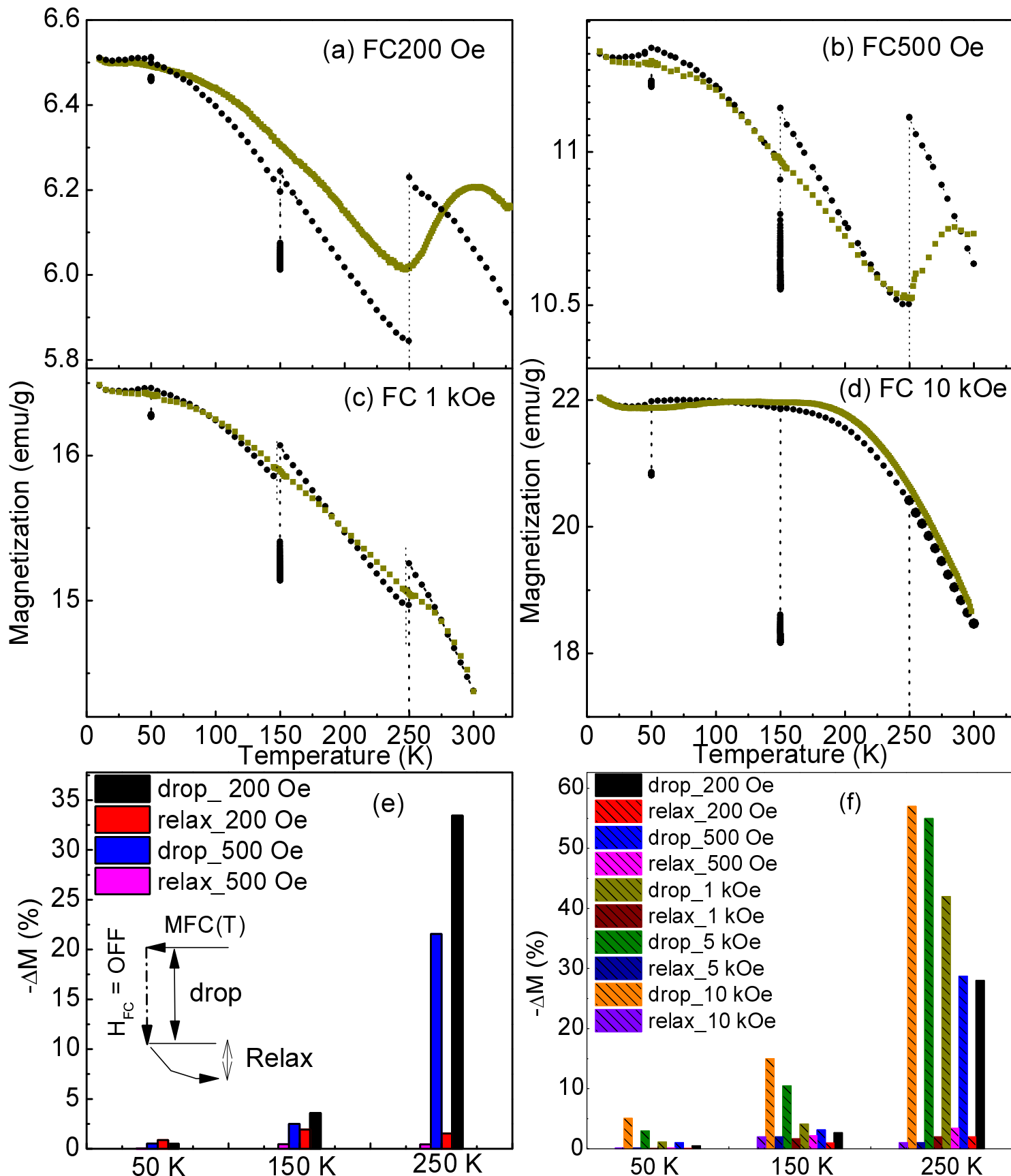


Fig. 8 MFCC(T) and MFCW(T) curves (a-d) of the CF80_BTO composite at selected magnetic fields with field OFF at 250 K, 150 K and 50 K during FCC mode and field continuity in FCW mode (a-d). The drop and relaxation of magnetization in field OFF condition, as sketched in the inset of (e), at 250 K, 150 K and 50 K are compared in bar diagram for CF90 sample (e) and CF80_BTO composite sample (f).

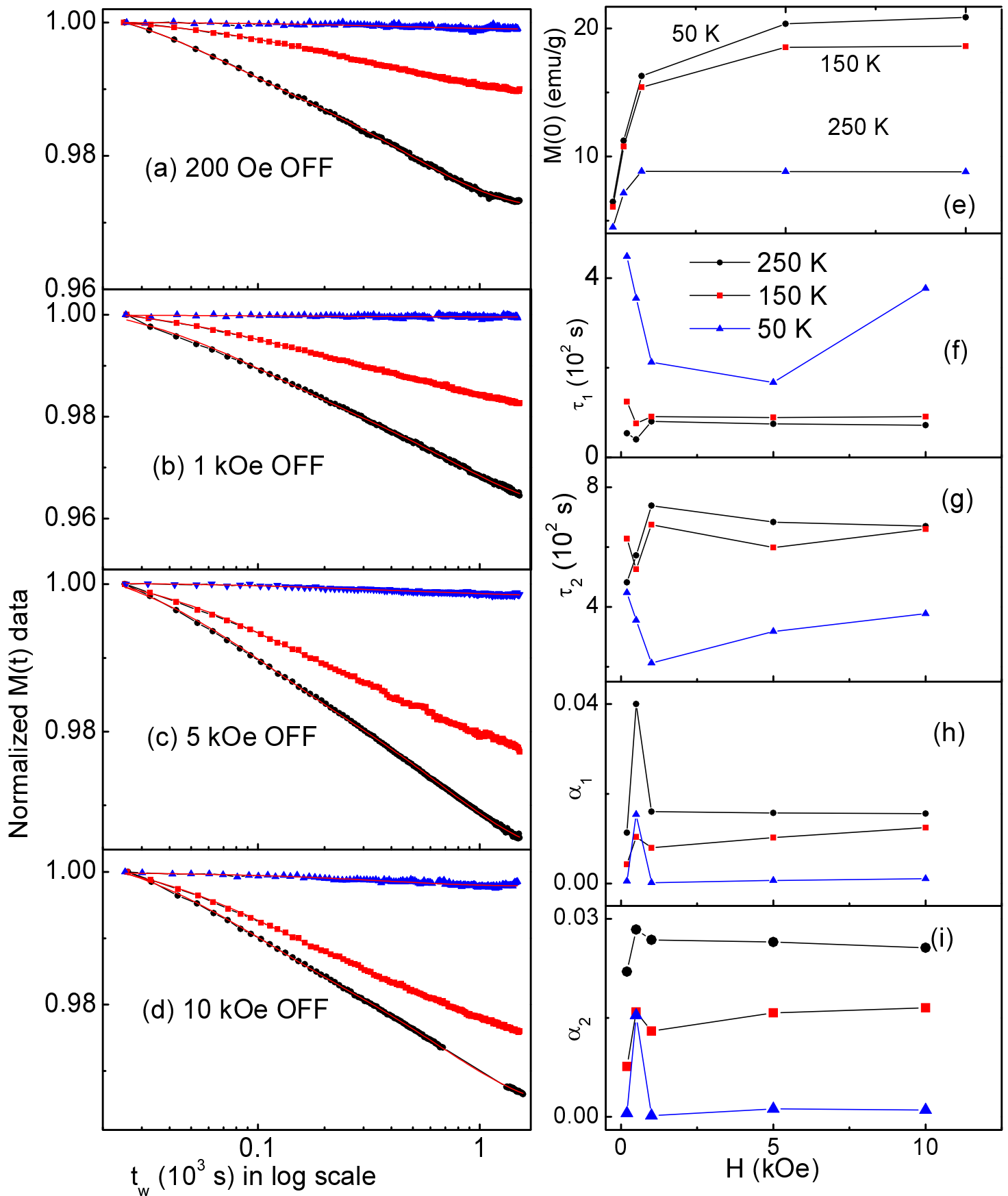


Fig. 9 Fit of the normalized $M(t_w)$ data of the composite sample(a-d), recorded at field OFF condition during MFCC(T) measurement, using equation (1). The fit parameters are shown in (e-i).

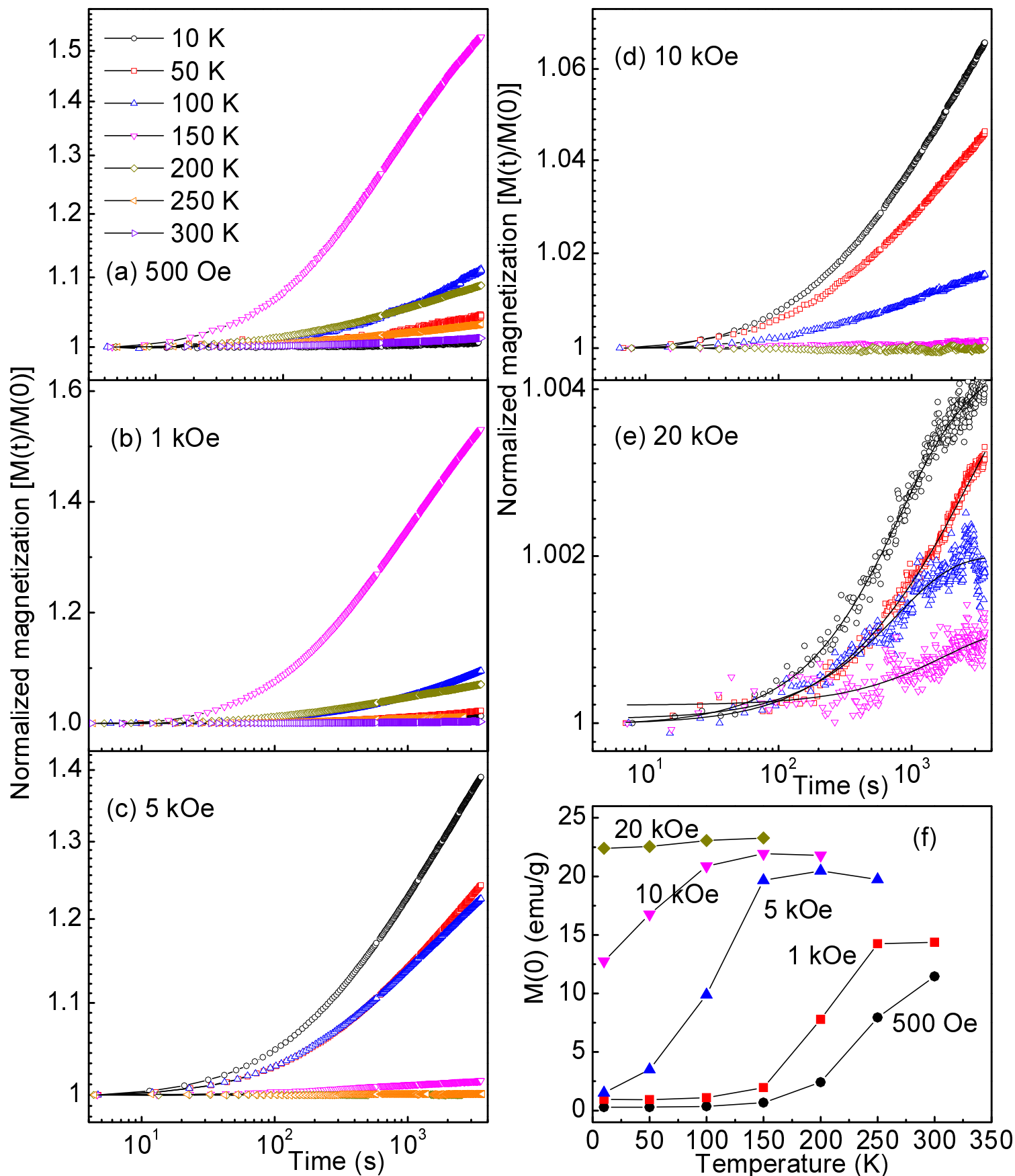


Fig. 10 Time dependence of normalized magnetization at different temperatures under constant magnetic fields (a-e) and (f) shows the magnetization used for normalization. The $M(t)$ data were fitted by power law with two time constants (τ_1 , τ_2).

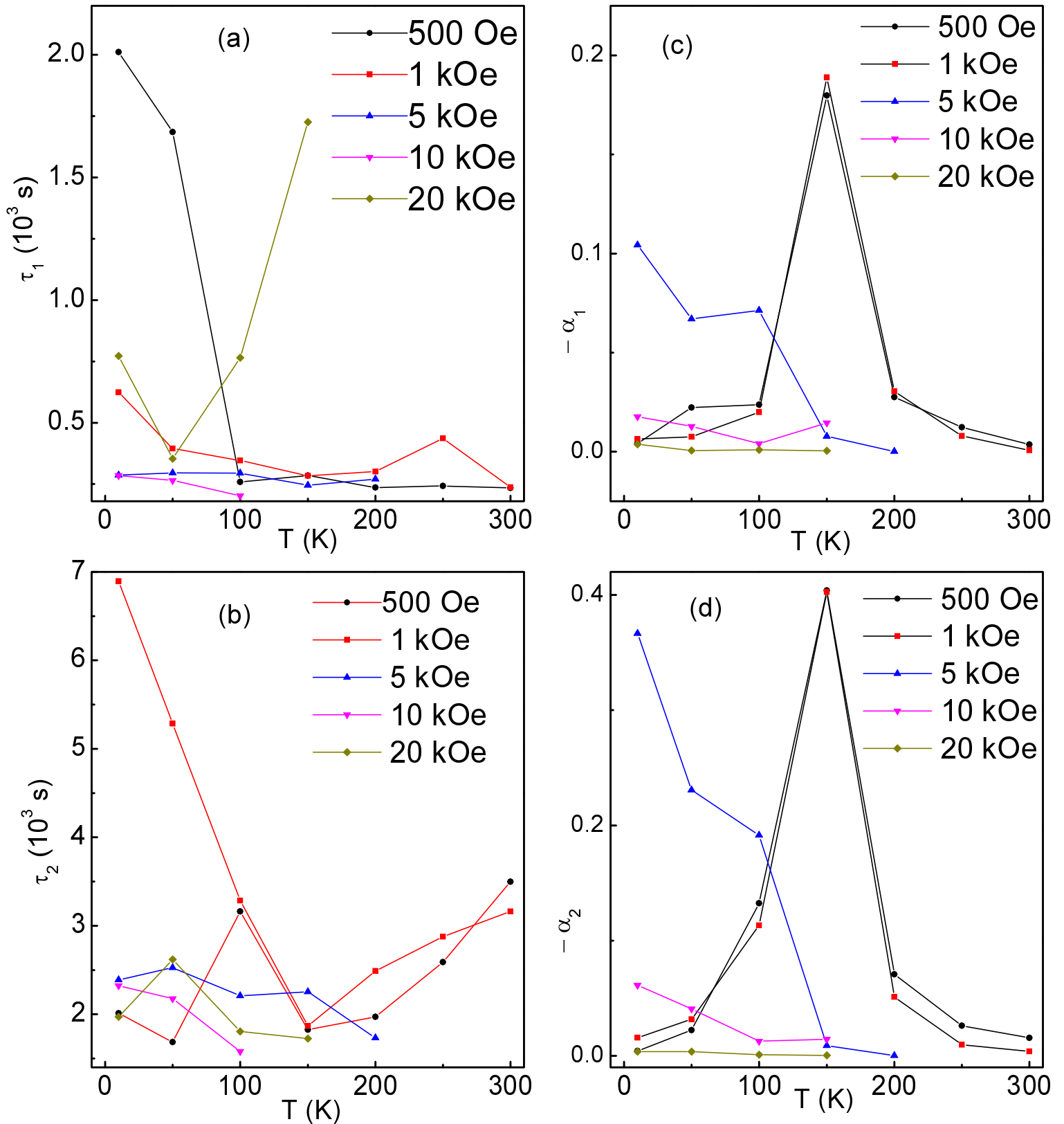


Fig. 11 Temperature variation of the fit parameters (τ_1 , τ_2 , α_1 and α_2) obtained by fitting of the in-field $M(t)$ curves of the CF80_BTO composite sample using exponential equation.

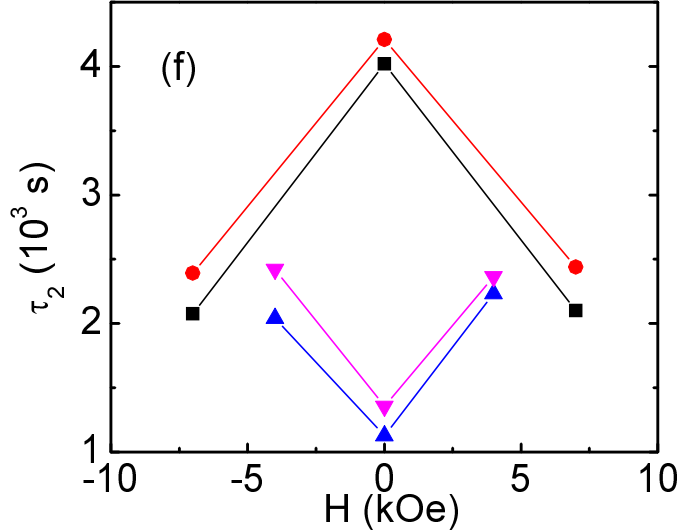
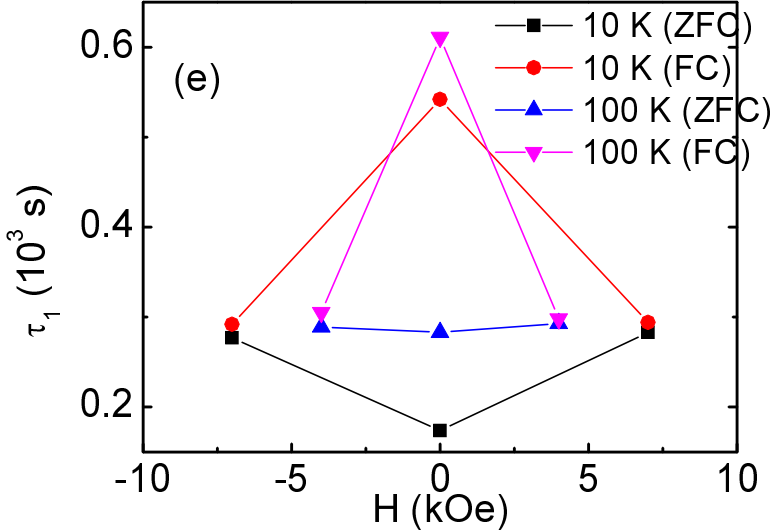
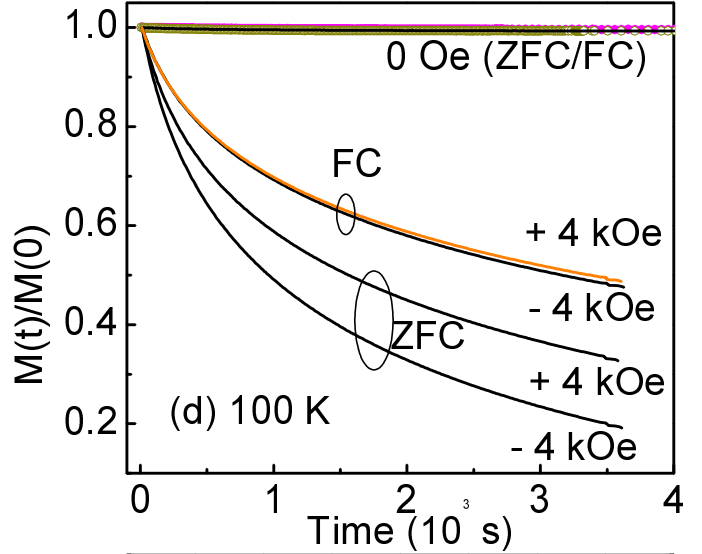
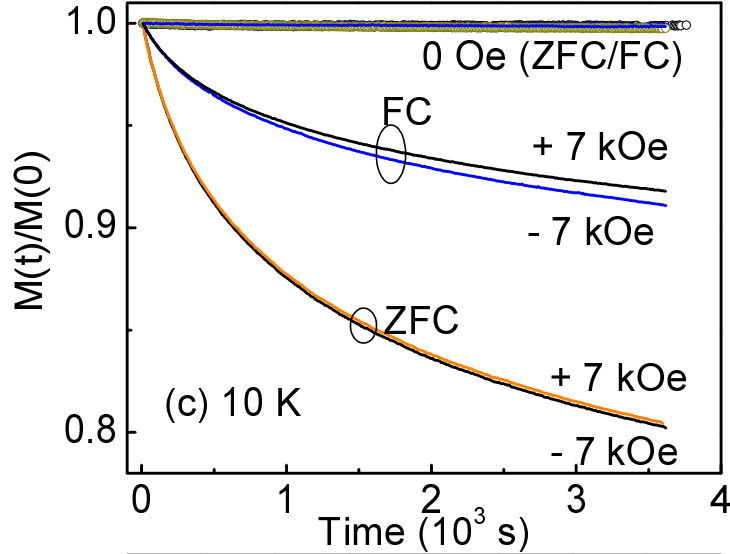
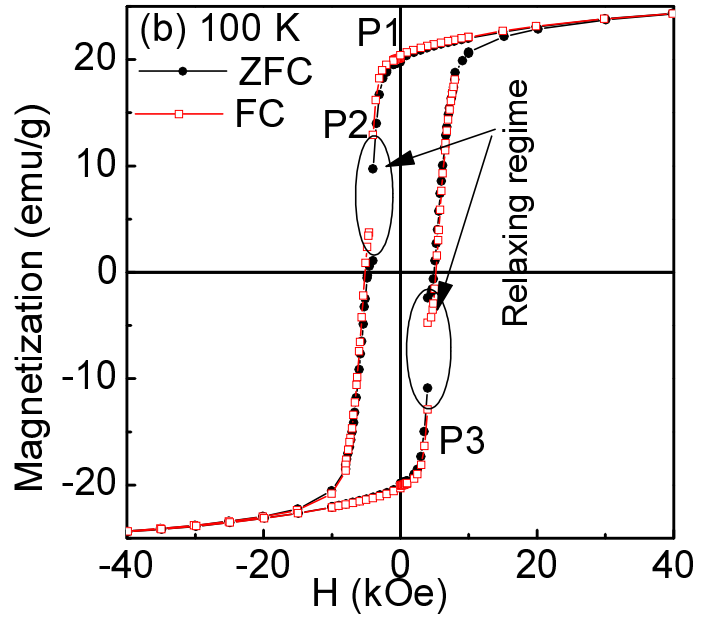
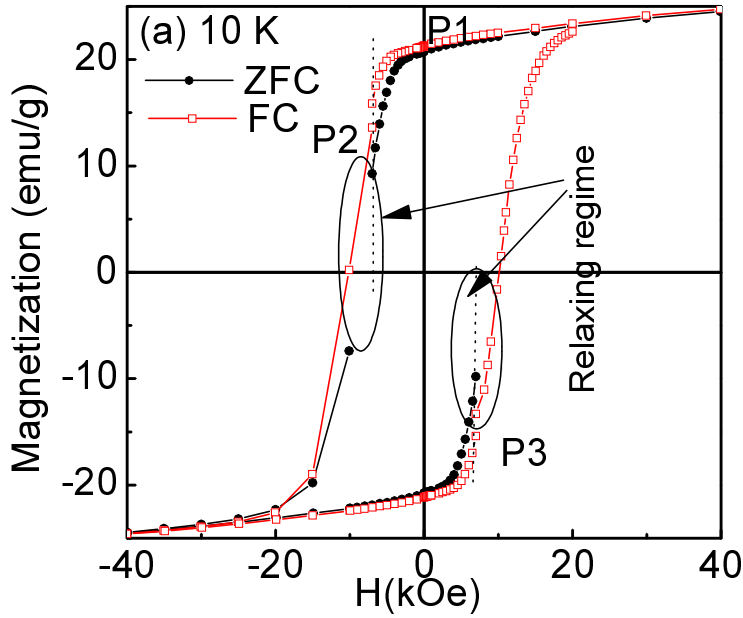


Fig. 12 ZFC and FC loop at 10 K (a) and 100 K (b) with intermediate waiting ftime 1 hr for recording $M(t)$ data at points P1, P2 and P3 while field was cycling. The $M(t)$ data (normalized) at 10 K (c) and 100 K(d) were fitted by power law with two time constants (τ_1 and τ_2). The fit values of τ_1 (e) and τ_2 (f) are plotted with constant measurement fields.

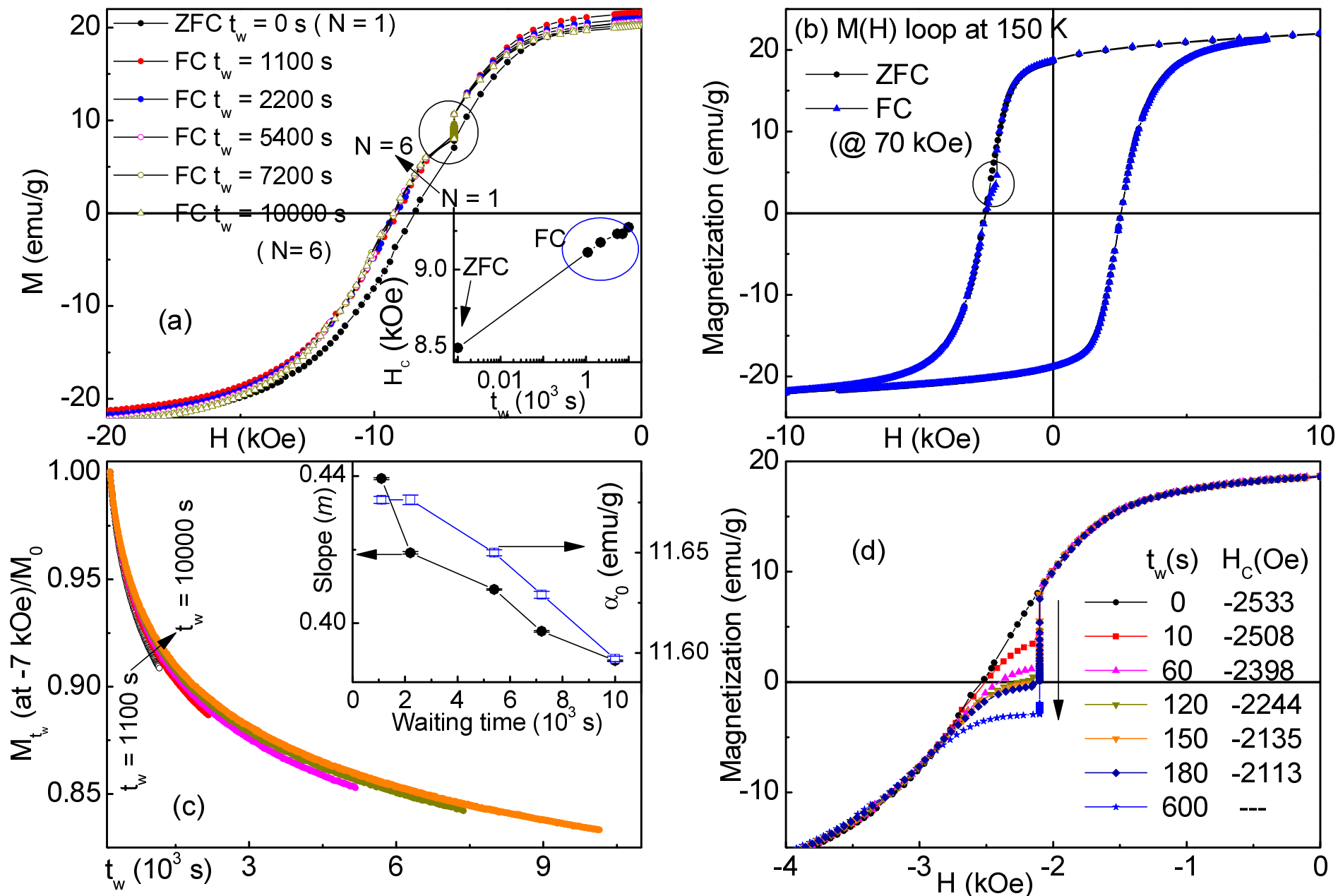


Fig. 13 M-H curves at 10 K under ZFC and FC modes (a). In FC mode, the $M(t_w)$ curves were recorded at -7 kOe, where t_w affected on FC coercivity (inset of a). Similar measurements of $M(H)$ curves under ZFC and FC modes were carried out at 150 K for wait-in field -2100 Oe (b). The in-field $M(t_w)$ curves at 10 K are fitted with logarithmic decay function (c) with fit parameters (inset). The effect of t_w on FC-coercivity and $M(H)$ curves are shown in (d).

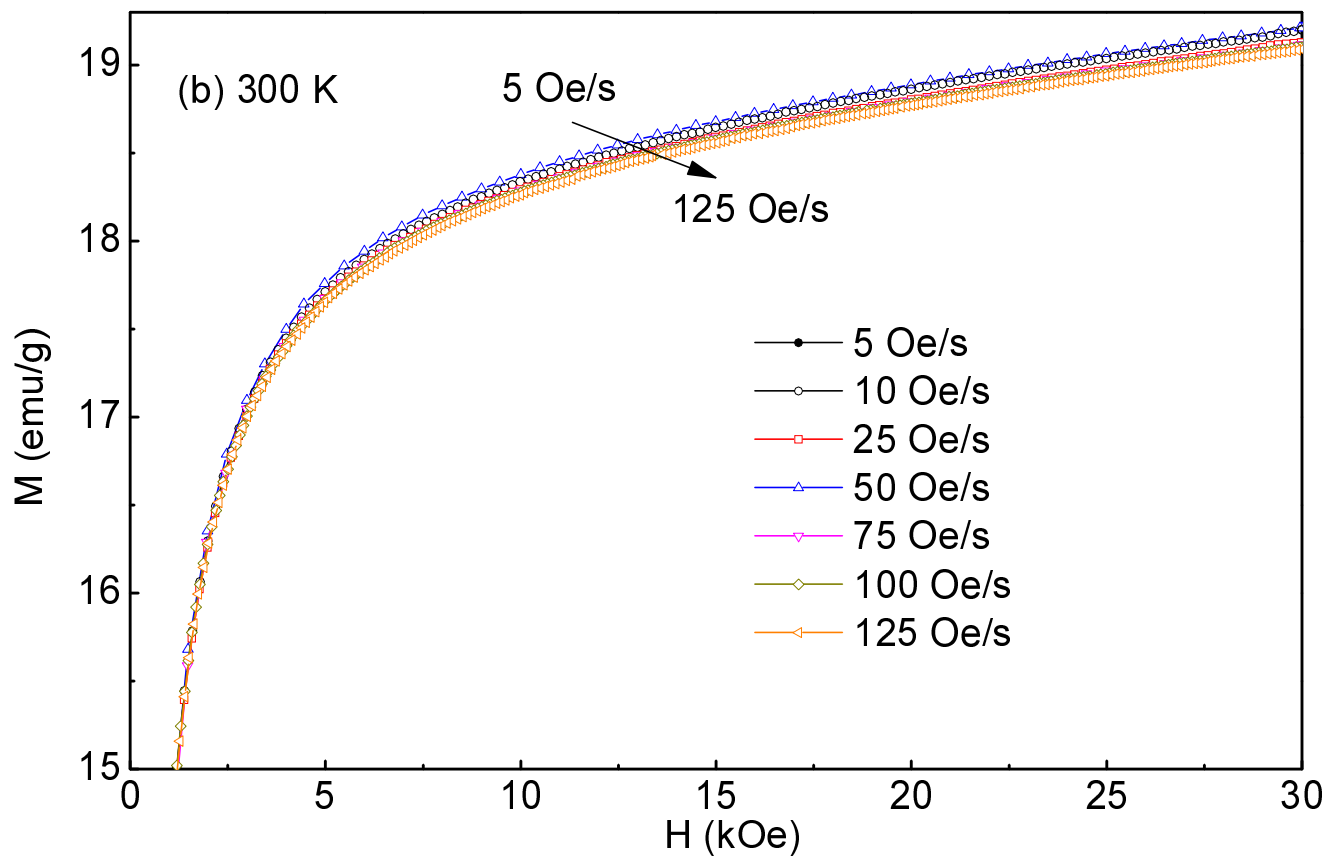
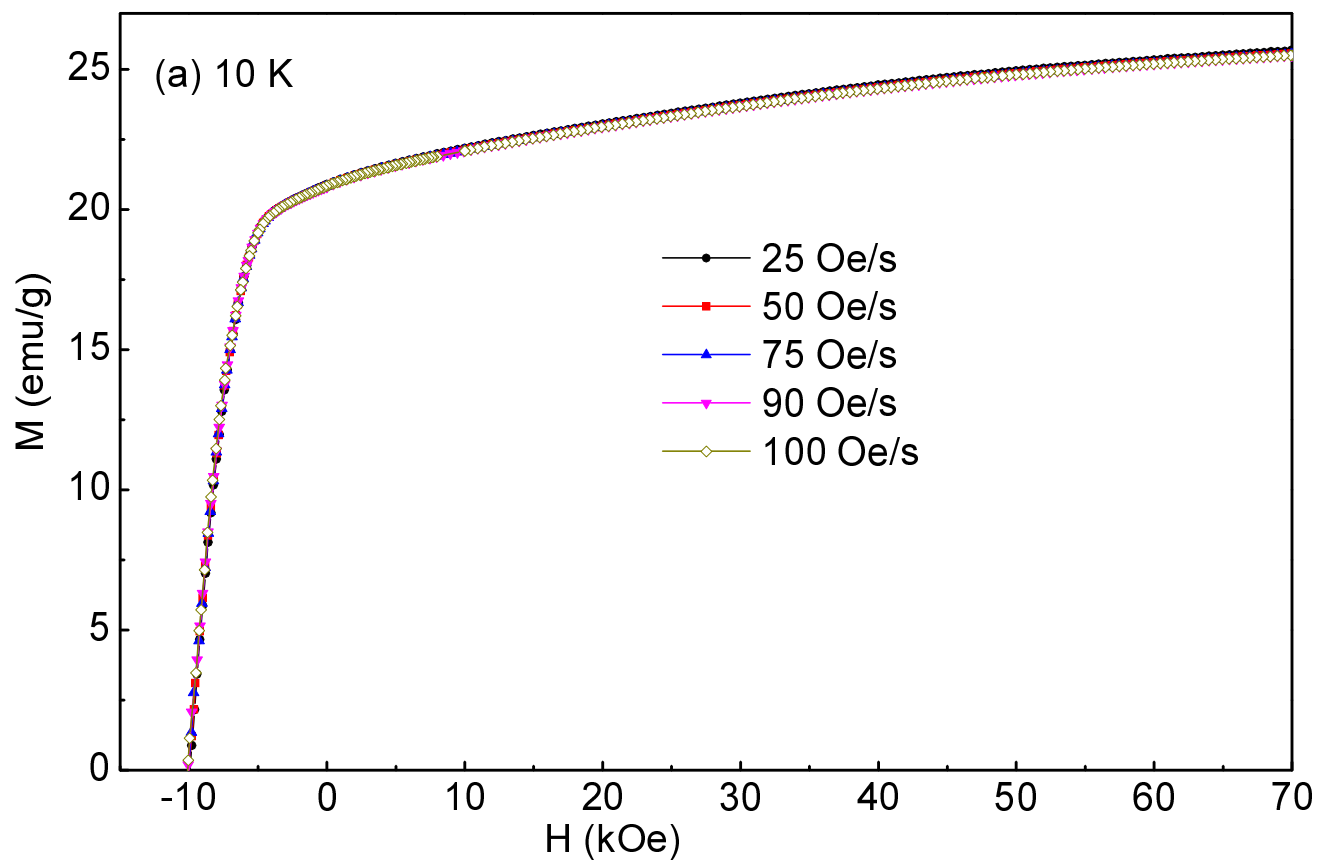


Fig. 14 M(H) curve measurement at 10 K (a) and 300 K (b) was repeated with different field sweeping rate for composite sample.